Vaal University of Technology
Your world to a better future
VUT

FACULTY OF APPLIED AND COMPUTER SCIENCES

DEPARTMENT OF CHEMISTRY

Antimicrobial activity and dye photodegradation of titanium dioxide nanoparticles immobilized on polyacrylonitrile-cellulose acetate polymer blended nanofibers

A dissertation submitted in fulfilment of the requirement for the degree of Magister Technologiae: Chemistry

Sibongile Chrestina Nkabinde

(Student number: 212112694)

Supervisor: Prof. M.J Moloto

Co-supervisor: Dr. K. P. Matabola (Mintek)

2019

Declaration

I, Sibongile Chrestina Nkabinde, present this dissertation as the work done by myself in fulfillment for a Magister Technologiae (MTech) degree in the Department of Chemistry, Vaal University of Technology, Andries Potgieter Blvd, Vanderbjalpark, 1900 under the supervision of Prof. M.J. Moloto and Co-supervision of Dr K.P. Matabola.

I therefore declare that this work has not been submitted in any other university.

Signature:…… Date:……..

Dedication

This reseach work is dedicated to my parents Busisiwe Nkabinde (Mother) and Piet Nkabinde (Father) for their love, support and prayers. My siblings, Simphiwe, Sarah, Thomas, Tsepo, Hlengiwe, Musa and my Grandparents for their love and support throughout my studies. I am heartily thankful for their lives.

Acknowledgements

I would firstly like to thank the Almighty mighty God, my heavenly father for my life, giving me strength and wisdom to do this research work. I am truly thankful for His blessings upon my life.

I am sincerely greatful to my supervisor Prof. M.J Moloto for his unwavering support, guidance and insight throughout this research study. Thank you for believing in me and encouraging me from the early stage of writing my proposal to the final level of this work. I am thankful to my co-supervisor Dr. K.P Matabola (Mintek) for all the advice, guidance and making it possible for me to do some of my experiements at Mintek premises.

I would also like to express my heartfelt gratitude to the Department of Chemistry staff and colleagues for their support and genuine interest in my research work. I am heartily thankful to the NCAP group for their helpful discussions, assistance and guidance with my research work. To Mr Z. Nate and Ms D.S More I am greatful for all the advice, assistance and kindness you have shown me throughout my research study.

I would also like to extend my special thanks to the following people: Dr P. Nyamukamba for providing me with polyacrylonitrile and titanium tetrachloride. Dr O. Mapazi for providing me with cellulose acetate. I would also like to thank the following people from the biotechnology department for assisting me with the antibacterial study: Mr G. Mohlala and Ms M.E Sekulisa.

I am grateful to the Council of Scientific and Industrial Research (CSIR) and National Research Foundation (NRF) for funding and all the assistance. I would also like to extend my gratitude to Mintek for allowing me to do some of the experiement on their premises.

Lastly I would like to thank my Family and all my friends for the support, love, encouragement and believing in me. Thank you all for your part in my research journey.

Abstract

Electrospinning is a method that has gained more attention due to its capability in spinning a wide variety of polymeric fibers and nanoparticles embedded in polymer fibers. Polymer blending has been considered the most appropriate way for creating new materials with fused properties which improve poor chemical, mechanical, thermal and dynamic mechanical properties of each polymer. Hence, in this study, electrospinning technique was used to fabricate polyacrylonitrile (PAN) nanofibers at concentrations of (10, 12 and 14 wt%) and cellulose acetate (CA) nanofibers at concentrations of (14, 16 and 18 wt%). 10wt% of PAN and 16 wt% of CA were blended together and the optimum blend ratio was found to be 80/20 PAN/CA. TiO_2 nanoparticles (0.2 and 0.4 wt%) were incorporated into CA nanofibers and (1, 2 and 3 wt%) were incorporated into PAN and PAN/CA blended polymers, respectively. Applied voltages of 20, 22 and 24 kV were varied at a spinning distance of 15cm and the optimum voltage for the fabrication of composite was 22 kV. The sol-gel method was used to synthesise the TiO_2 nanoparticles at different calcination temperatures of 400, 500 and 600 ºC. The fabricated composite nanofibers were tested for antibacterial and photocatalytic activities. The synthesised nanomaterials were characterized using SEM, TEM, EDX, UV-Vis, PL, FTIR spectroscopy, XRD and TGA. The absorption and emission spectra illustrated the formation of TiO_2 nanoparticles and the increase in absorption band edges. TEM showed the spherical morphology of the nanoparticles with average diameter of 12.2 nm for nanoparticles calcined at 500 ºC. SEM illustrated the diameter and morphology of the nanofibers and composites with the average diameter of 220, 338, 181, 250, 538, 294 nm for PAN, CA, PAN-TiO_2, CA-TiO_2, PAN/CA and PAN/CA-TiO_2, respectively. XRD revealed anatase phase as the dominant crystalline phase of the synthesised nanoparticles. FTIR spectroscopy and EDX signified that the formation of composite nanofibers and the presence of TiO_2 nanoparticles corresponded to the Ti-O stretching and Ti-O-Ti bands on the FTIR spectra. The antimicrobial activity of the composite nanofibers were tested against *E. coli*, *S. aureus* and *C. albicans* microorganisms. The photocatalytic activity of the nanomaterials was tested using methyl orange dye. PAN/CA-TiO_2 composite nanofibers revealed the greatest antibacterial activity against selected microorganisms as compared to the other nanocomposites. PAN/CA-TiO_2 nanocomposite (44%) showed greater rate of photodegradation of methyl orange than PAN-TiO_2 nanofibers (28%) and TiO_2 nanoparticles (12%) under visible light irradiation.

Table of contents

List of Figures

List of Tables

List of Abbreviations

Ag/N-doped: Silver nitrogen doped

C. albicans: Candida albicans

CNFs: Carbon nanofibers

CNTs: Carbon nanotubes

CA: Cellulose acetate

CVD: Chemical vapour deposition

CB: Conductive band

CFU: Colony forming unit

DTA: Diffractctional thermal analysis

DMAc: N,N-Dimethylacetamide

E. coli: Escherichia coli

EDX: Energy dispersive X-ray spectroscopy

FTIR: Fourier-transform infrared spectroscopy

MO: Methyl orange

NP's: Nanoparticles

N-doped: nitrogen doped

OD: Optical density

PL: Photoluminescence

PAN: Polyacrylonitrile

PANI: Polyaniline

PVA: Poly vinyl alcohol

PVC: Poly (vinyl chloride)

PLLA: Poly-L-lactide

RBC: regenerated bacterial cellulose

SEM: Scanning electron microscopy

S. aureus: Staphylococcus aureus

TEM: Transmission electron microscopy

TGA: Thermogravimetric analysis

UV-Vis: Ultraviolet visible

VB: Valence band

XRD: X-ray diffraction

Dissertation outline

This dissertation from the research study is comprised of 4 chapters. Chapter 1 is the introduction of the research study, which introduce the research by giving a broad overview about nanoparticles and polymer fibers as a possible solution to world problems associated bacteria found in contaminated water. This chapter also outlines the literature review of the research study, which gives a review of titanium dioxide nanoparticles, its properties and applications. In this chapter methods for the synthesis of nanoparticles were discussed and the sol-gel method as the one used in this study for the preparation of TiO_2 nanoparticles. Furthermore, this chapter outlines the synthesis of polymer blended fibers and the immobilization of TiO_2 nanoparticles on polymer support using the electrospinning technique. The chapter is ended by giving the problem statement, research aims and objectives. Chapter 2 is composed of the experimental part of the study which describes the methods used for the synthesis to TiO_2 nanoparticles and immobilization of TiO_2 nanoparticles onto the polyacrylonitrile/cellulose acetate polymer blended nanofibers by electrospinning. Characterizations techniques for this study were discussed. The chapter ends by describing the methods for the antibacterial and photocatalytic activity. The results are presented and discussed in Chapter 3 and in Chapter 4 a concluding summary is given with suggestions for further work and recommendations. Finally, the reference list for chapter one, two, three and four is at the end of the whole document.

CHAPTER 1:
BACKGROUND AND LITERATURE REVIEW

1. Nanotechnology

Nanoscale materials have attracted more attention in the science and research world. A nanometer is a unit of length equal to one billionth of a meter. In recent years, scientists have gained more interest in manufacturing new improved materials at nanoscale level (Hayle & Gonfa 2014). Nanotechnology, is considered an emerging division of technology with the ability to manipulate materials shape and size into nanoscale level. Nanomaterials are significant subset of nanotechnology with unique superior properties which differ from materials in molecular form, these include the physical and chemical properties, also high surface area to volume ratio than their conventional forms (Sabriye et al., 2013; Morteza et al., 2012). These materials with improved properties can be applied in chemical reactions, enhance the performance of medical devices, drug delivery systems and energy storage (Rizwan et al., 2014). Nanomaterials can be classified as zero-dimensional nanomaterials (i.e. nanoparticles, nanoclusters and nanodots), one-dimensional nanomaterials (i.e. nanofibers, nanotubes and nanowires) and two-dimensional nanomatierals (i.e. nanoplatelets and nanofilms) (Khan et al., 2017). Part of the nanoscale materials include the polymer nanofibers, which are defined as fiber materials with a diameter in nanometer range. Nanofibers are classified as both natural and synthetic polymer nanofibers, hence they exhibit different properties which make them favorable for many applications. They are favoured accounting to their high surface-to-volume ratio, mechanical strength, light weight and controllable pore structures. These remarkable properties make the polymer nanofibers favovourable for application in fields such as air fitration, tissue engineering, materials development, sensors and drug delivery (Tang et al., 2016)

Exceedingly tiny particles called nanoparticles are the first-generation outcomes of nanotechnology and have one dimension less than 100 nm at least (Watanabe et al., 2013). Nanoparticles are made up of carbon, metal chalcogenides or organic matter and have different shape, size and structure. These different shapes include cylindrical, spherical, flat, tubular, etc. or irregular and the surface can be uniform or irregular (Anu & Saravanakumar 2017; Khan et al.,

2017). Nanoparticles exhibit unique chemical and size-related properties allied with their large surface area and discontinuous properties (quantum confinement), which allow these materials to be applicable in different fields (Watanabe et al., 2013). In relation to these nanostructures, metal and metal oxide-based nanoparticles such as nickel, copper, zinc, silver, and titanium are considered as promising nanomaterial due to their antibacterial properties and the ability to degrade contaminants in wastewater. Some natural and synthetic nanomaterials that have strong antibacterial properties include silver nanoparticles, chitosan, photocatalytic TiO_2 and carbon nanotubes (CNTs). Among these nanomaterials, titanium dioxide (TiO_2) has been reported as the most efficient nanomaterial in various areas ranging from wastewater and air treatment to self-cleaning surfaces due to its strong oxidizing power, high photo stability, economical, nontoxicity, antimicrobial properties and redox selectivity (Sharmila et al., 2013; Huei-Siou et al., 2011). With these properties, titanium dioxide (TiO_2) nanoparticles have been considered in meeting the raising demands for the development of safe, low cost and effective bioactive compounds for the problem of microbial resistance (Razi & Meryam 2013).

Various methods have been used for the synthesis of nanoparticles that are categorized into bottom-up or top-down method. Table 1 shows the categories of the nanoparticles synthesised from various methods. The bottom-up or constructive method is based on the synthesis of nanoparticles from atom to cluster to nanoparticles. The top-down or destructive method is reduction of a bulk material to nanometric scale particle. The bottom-up method includes sol-gel, chemical vapour deposition and biosynthesis. Among these, sol-gel method has been an attractive method for the synthesis of nanoparticles due to its simplicity, low cost and the production of desirable structural characteristics of the nanoparticles such as grain size, particle morphology and porosity (Sharmila et al., 2013). The synthesis of TiO_2 using the sol-gel method involves the hydrolysis and polycondensation of metal alkoxides. The amount of water, the type of metal alkoxide and the catalyst used in the sol-gel method are the main parameters that regulate the physical properties of the synthesised TiO_2 nanoparticles (Dubey 2017). Normally, most products obtained via sol-gel method are amorphous, hence, posttreatment such as the calcination method is preferred to modify the crystal phase, particle size, specific surface area and morphology of TiO_2 nanoparticles for different applications (Wetchakun et al., 2012; Wang et al., 2011).

Though TiO_2 is efficient, complications arise when used in powdered form due to filtration problems allied with the small size of the particles resulting in the reduction of the quantum efficiency. This is as a result of the recombination of the photo-generated holes and electrons, the difficulty in the removal and reuse of the photocatalyst in water treatment and its limitation to utilize visible light due to its wide band gap (~3.2 eV) (Nyamukamba et al., 2016). These complications have a poor influence on the economy and human health. Several procedures have been applied to enhance the photocatalytic and antimicrobial properties of TiO_2 in order to allow the use of visible light, easy isolation and reuse of the photocatalyst.

Table 1. Categories of the nanoparticles synthesised from different methods

Category	Method	Nanoparticles
Bottom-up	Sol-gel	Carbon, metal and metal oxide based
	Spinning	Organic polymer
	Chemical Vapour Deposition (CVD)	Carbon and metal based
	Biosynthesis	Carbon and metal oxide based
		Organic polymers and metal based
Top-Bottom	Mechanical milling	Metal, oxide and polymer based
	Nanolithography	Metal based
	Laser ablation	Carbon based and metal oxide based
	Sputtering	Metal based
	Thermal decomposition	Carbon and metal oxide based

Among these procedures, immobilization of TiO_2 nanoparticles on the polymer blends support is highly significant. Immobilization of TiO_2 has the benefit of high quantum utilization efficiency than TiO_2 photocatalyst in powder form and has been reported to reduce the cost of filtration of dispersed nanoparticles after the process of treating polluted water with the powdered photocatalyst (Seema et al, 2013). Hence, this study aims to immobilize TiO_2 nanoparticles on

substrate polymer blend of polyacrylonitrile (PAN) and cellulose acetate (CA) to enhance the reuse of the photocatalyst and improve antimicrobial properties.

Polyacrylonitrile is a synthetic semi-crystalline polymer that has shown superior performance in a wide range of applications due to its high mechanical properties, thermal stability and chemical resistance (Shi et al., 2015). The combinations of synthetic and neutral polymers is an effective way of enhancing the properties of the individual polymers and also of TiO_2 nanoparticles that will be incorporated on the polymer blend. Furthermore, cellulose acetate (CA) is a typical neutral polymer, it is a by-product of natural polymer cellulose with good characteristics of thermal stability, chemical resistance, mechanical strength and good solubility in organic solvents which makes cellulose acetate outstanding for electrospinning (Se Wook et al., 2015). In the company of different techniques employed to produce fibers, electrospinning is favoured because of its ability of fabricating fibers with diameters in micro-meter scale and small diameter (nanofibers). Nanofibers produced via electrospinning possess a high surface area to volume ratio and found application in different areas such as bioengineering, nanocatalysis, filtration and electronics (Haider et al., 2018; More et al., 2015).

This study looks at the synthesis of TiO_2 nanoparticles using the sol-gel method and varying the calcination temperatures of the nanoparticles to modify the crystyal phase, diameter and mopholgical properties of the TiO_2 nanoparticles. The polymer nanofibers, polymer blended nanofibers and composite nanofibers are also discussed. Furthermore, the electrospinning fundamentals and process, factors influencing the electrospinning process and the relationship between the processing parameters during electrosping and morphology are also studied.

1.1. Titanium dioxide nanoparticles

Metal nanomaterials have become an interesting class of materials due to their intrinsic properties and potential application in diverse fields including catalysis, magnetic recording media, microelectronics and medicine. Among them, TiO_2 is a nanomaterial that has been explored and has gained more interest amongst researchers around the world. It belongs to the family of transition metal oxides and exists in both crystalline and amorphous forms. Moreover, it is found in nature in three crystalline polymorphs (Figure 1.1), namely: anatase (tetragonal), brookite

(orthorhombic) and rutile (tetragonal) (Sharmila et al., 2013). These polymorphs reveal different properties and different photocatalytic performances. Rutile is the stable phase while both anatase and brookite are metastable. Titania undergoes irreversibly transformation phase from anatase to rutile through its exposure to high temperature heating ranging between 600-800 ºC. The anatase phase is preferred over other polymorphs because it is more active than rutile and has greater photocatalytic activity and potential application in fields such as air purification, water treatment and biomedicine (Gupta & Tripathi, 2011). Various investigations have established that TiO_2 possess different mechanical, chemical and optical properties in the form of nanoparticles compared to their bulk counterparts and are much more effective and efficient as a photocatalyst.

The antibacterial and antifungal effects of TiO_2 nanoparticles has the great ability to kill a wide number of microorganisms such as *Escherichia coli (E. coli)*, *Staphylococcus aureus (S. aureus)* and *Candida albicans* (*C. albicans*). Microorganisms can be inactivated by TiO_2 upon irradiation with light energy equivalent to or greater than its band gap energy, the electron is excited from the valence band (VB) to conduction band (CB) (Haoran et al., 2015). The photocatalytic properties are derived from formation of photo generated charge carries hole and electron (h+/e-), which occurs upon the absorption of UV light corresponding to the band gap. The photo-generated holes in the valence band migrate to the surface of TiO_2 particles and serving as redox sources that can react with adsorbed water molecules, leading to the formation of hydroxyl radicals (•OH).

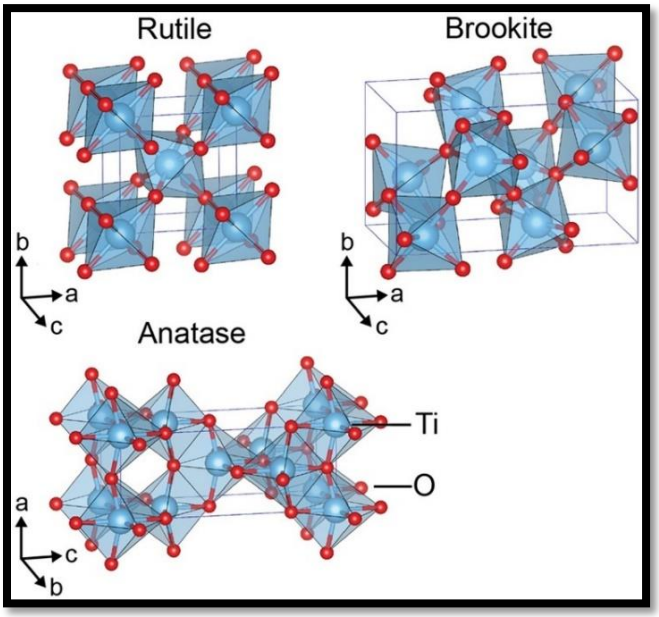

Figure 1.1: Three polymorphs of TiO_2 (Antase, Rutile & Brokite) (Haggerty et al., 2017).

The active holes and hydroxyl radicals oxidize organic compounds in aqueous solution on the TiO_2 surface.On the other hand, electrons in the conduction band participate in reduction reactions, which typically react with molecular oxygen in air to produce superoxide radical anions ($O_2^{\bullet -}$) (Nakata & Fujishima, 2012). The produced hydroxyl radicals and superoxide radicals irradiated on the TiO_2 surface have the ability to kill microorganisms. Therefore, the utilisation of TiO_2 particles in nanometer size is more effective and has the capacity to increase the antimicrobial activity of TiO_2. Ahmad & Sardar (2013) synthesised anatase TiO_2 nanoparticles using the sol-gel method and investigated its antibacterial activity against *E. coli* strain. TiO_2 nanoparticles showed inhibitory effect on the growth of *E. coli* strain, hence, TiO_2 nanoparticles can be considered as potent antibacterial compound. Sabriye et al, (2013) investigated antimicrobial activity of synthesised TiO_2 nanoparticles against *E. coli* and *S. aureus*. The synthesised TiO_2 nanoparticles showed strong antibacterial activity against the later bacteria.

1.1.1. Methods for synthesis of nanoparticles

With the emergence of nanotechnology-based materials research, scientists have gained more interest in the development of improved methods for the fabrication of nanoparticles. The synthesis methods for nanoparticles are divided into three main groups, physical (gas condensation and physical vapour deposition), chemical (hydrothermal technique and sol-gel synthesis) and biological (green synthesis) methods (Iravani et al., 2014). The synthesis methods are improved or developed to reduce the production cost and improve the properties of the nanoparticles. The unique properties of nanoparticles are dependent on the size, morphology, particle dispersing without agglomeration and the synthesis method. (Namita, 2015).

(a) Gas condensation Technique

Gas condensation is one of the physical method for synthesis of metal and metal oxide nanoparticles. This physical method operates in the absence of a solvent contaminant in the preparation of thin films and uniform nanoparticles, which is one of the advantages of this method (Iravani et al., 2014). Gas condensation was the first technique used to synthesise nanocrystalline metals and alloys. This method has capability of directly synthesising high purity and crystalline nanoparticles with relatively high production rate (Azin et al., 2016). The scale-up of the gas

condensation method is suitable for industrial production but has some limitations to a laboratory scale (Namita, 2015). With gas condensation method, high residual gas pressure causes the production of ultrafine particles by gas phase collision. The ultrafine particles are formed by collision of evaporated atoms with residual gas molecules. A convective flow of inert gass transports the nanoparticles formed over the evaporation source via thermophoresis towards a substrate with a liquid nitrogen cool surface (Namita, 2015; Azin et al., 2016).

(b) Sol-gel Technique

During the sol-gel process, nanomaterials are formed by means of polycondensation reaction of monomers into colloidal solution which evolves into an integrated web of nanoparticles or bulk polymerized network. Different precursors can be utilized for this kind of reaction, however, the metal alkoxides or chloride salts are widely used (Nistico et al., 2017). Alkoxides are metallic precursors for silica, titanium, aluminium and are immiscible in water. Sol-gel process takes place in four typical stages which are hydrolysis, condensation, growth of particles and agglomeration of particle (Namita, 2015). There are two routes for the sol-gel method, the aqueous sol-gel which uses water as the reaction medium and the nonaqueous sol-gel which uses organic solvents as the reaction medium. In the aqueous sol-gel method the oxygen is supplied by the water solvent which is necessary for the formation of metal oxide (Rao et al., 2017). When using sol-gel process, there are several parameters that need to be considered during the synthesis to produce nanoparticles with desired properties. These are, thermal treatment, cooling rate and water content to keep away from undesirable effects (Nistico et al., 2017). The sol-gel technique has been favourable to most research studies because of its low processing cost, high productivity, rapid productivity of fine homogeneous powder and energy efficiency (Ramesh, 2013). Nithya et al., (2018) investigated the photocatalytic and antibacterial activity of neodymium doped TiO_2 nanoparticles by sol-gel method. The Nd doped TiO_2 nanoparticles exhibited good photocatalytic and antibacterial activities. The chemical approach using sol-gel technique will be used in this study for the synthesis of titanium dioxide nanoparticles due to its simplicity and convenience. Moreover, parameters such as average crystallite size, morphology and surface area are controlled when calcining the nanoparticles to determine photocatalytic activity of TiO_2.

1.1.2. Application of TiO_2 nanoparticles

Titanium dioxide (TiO_2) attracted a great deal in self-cleaning, wastewater treatment, degrading of pesticides and production of hydrogen fuel because it exhibits good optical, dielectric and photocatalytic properties from size quantization (Gupta & Tripathi, 2011; Sabriye et al., 2013). Moreover, TiO_2 can be supported on different substrates to enhance its ability to mineralize organic pollutants (Seema et al., 2013).

- **Degradation of pesticides and organic pollutants:** Pesticides (herbicides, insecticides and fungicides) are toxic substances released purposely into the environment to kill specific pests, fungal diseases and weeds. When pesticides cause contamination in aquatic environment, they have drawbacks of toxicity to human beings and other organisms (Gupta & Tripathi, 2011). Also the release of dangerous industrial organic pollutants into water posses health risks to human and animals. Therefore, TiO_2 is utilized for environmental clean-up of organic pollutants through photo oxidation because of it's efficiency in the degradation of organic pollutants (including organic dyes) in water (Hir et al., 2017).
- **Photo induced hydrophilic coatings and self-cleaning devices:** The demand of cleaning the surface of buildings is due to the exposure of the building to dirt, soot, vehicles and other particulates. Organisms such as bacteria, algae and fungi that grow on the surface of the building result in the damage of the building exterior. Therefore, to prevent this problem, TiO_2 is used as a photocatalyst for coating buildings and serves the purpose of self-cleaning (Gupta & Tripathi, 2011).
- **Wastewater treatment:** Lack of fresh water is one of the major challenges that the world is facing. Drinking water polluted with viruses and bacteria is a threat to human health and living organisms. Titanium dioxide (TiO_2) nanoparticles has been reported as the most efficient nanomaterial for wastewater treatment and disinfection due to its strong oxidizing power, high photostability, economical, non-toxic, antimicrobial properties and redox selectivity (Huei-Siou et al., 2011). TiO_2 nanoparticles have been useful in degrading pollutants in wastewater and shows great ability of killing both gram negative and gram positive bacteria as well as a variety of viruses (Gupta & Tripathi, 2011).
- **Other applications include:** making of cosmetic products such as whitening creams, sunscreens creams and skin milks. They also find use in paper industry for improving opacity of paper.

1.2. Polymer nanofibers

Natural and synthetic polymers are created via polymerization of many small molecules known as monomers. Polymer fibers are subset of man-made fibers for they do not come from natural materials, they are chemically synthesised. Structured polymer nanofibers are produced using electrospinning technique as it shows to be an excellent method for production of polymer nanofibers using different solvents. The diameter of polymer nanofibers range from a few nanometers to ten of macrometers (Silke, 2002). The scientific world has taken advantage of the versatility of polymers nanofibers as they are applicable in a broad range of areas such as biomedical application, fiber templates for the preparation of functional nanotubes, thin fibers for filter application and as reinforcing components in composite systems. They have high specific surface-to-area properties compared to other conventional materials and have the advantages of low cost, ease to process and good productivity (Bognitzki et al., 2001).

1.2.1. Polymer blended fibers

Blending has been considered the most appropriate way for creating new materials with fused properties which improve poor chemical, mechanical, thermal and dynamic mechanical properties of each polymer. Polymer blend is a mixture of at least two or more polymers without changing their individual properties resulting in new bicomponent fibers with unique and improved properties (Jyotishkumar et al., 2015). Attention has been focused more on the subject of polymer blended fibers both theoretical and experimental. Blending (Figure 1.2) is an easy and cost-effective method for developing polymeric materials that have the ability to adapt to many different

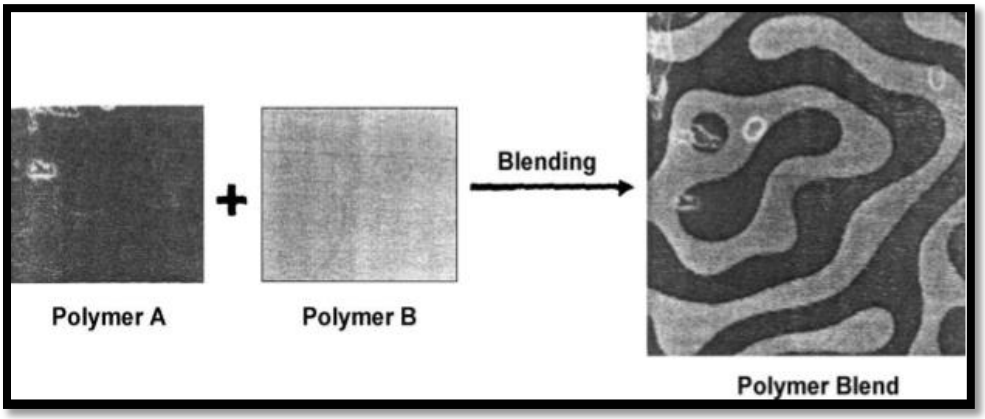

Figure 1.2: Schematic diagram showing two different polymers blended together (Ocwelwang et al., 2012).

applications. Furthermore, blending makes it possible for polymer wastes to be reused and recycled (Amoabeng et al., 2017). Among different methods used for the production of polymer blended fibers, electrospinning technique has been favoured due to its ability of producing fibres with diameters in nanometer range. Generally, there are two types of polymer blends, homogenous (miscible) and heterogenous (immiscible) blend. Majority of the polymer blends are immiscible due to the thermodynamics of the polymer blend and the kinetics of the mixing process resulting in a separated-phase morphology (Mofokeng, 2015). The size and morphology of dispersed phases of the blended polymers are established by conditions such as viscosity ratio, time, temperature and shear stress. Mahalingam et al., (2017) demonstrated the blend effect of polyacrylonitrile (PAN) and cellulose acetate (CA) which were subjected to gyration under pressure. They found that the PAN-CA blended fibers were longer and thicker than the fibers produced from pure PAN and CA. The PAN-CA blended fibers showed to have distinct layer structure made of several fibers stacked together in the upper and lower regions of the micrographs.

(a) Cellulose acetate

Cellulose is the most abundant natural organic polymer on earth. This raw material is characterized by its good flexibility, almost unlimitedly available, biodegradability, biocompatible, increased mechanical strength, chemical resistance, nontoxicity and low cost (Zizovica et al., 2018). It is described as an acetate ester of cellulose bonded either through the oxygen to the terminal carbon on the cellulose or oxygen bonded directly to the cellulose ring. Though cellulose has good characteristics, its drawback is poor ability of dissolving in most organic solvents due to its strong inter- and intra- molecular hydrogen bonding that are responsible for the hydrophilic nature of the biopolymer. Cellulose derivatives are used as a solution to this problem as they easily dissolve in organic solvents (Se wook et al., 2015). Cellulose acetate (CA) is one of the mostly used organic soluble derivatives. It is soluble in organic solvents and that makes it an outstanding material for electrospinning. Solvents used for fabrication of cellulose acetate nanofibers have influence on the morphology and diameter of the fibers. Single solvent systems are not suitable for producing uniform CA fibers. Therefore, in order to obtain uniform fibers, binary solvent systems are used in CA electrospinning. Mostly, the mixture of acetone/N,N-dimethylacetamide is the most appropriate solvent system for electrospinning of CA fibers (Matulevicius et al., 2014). Cellulose acetate shows good hydrolytic stability and can be recycled in environment by biodegradation. Electrospun CA fibers are characterized by several advantages which are the large specific area,

porosity of electrospun nanofibers, good thermal stability and chemical resistance (Goetz et al., 2015).

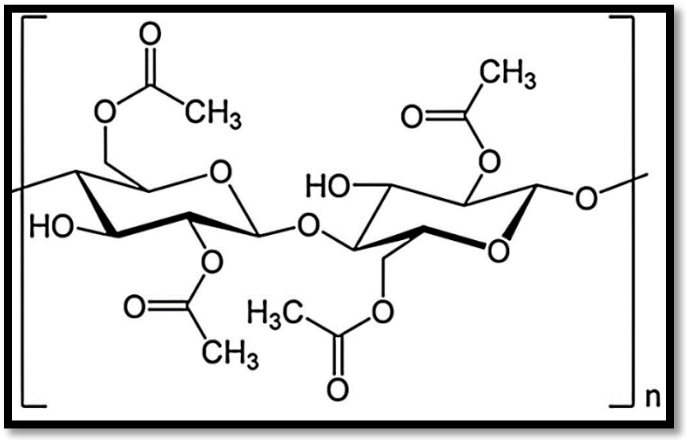

Figure 1.3: Chemical structure of cellulose acetate (Zizovica et al., 2018).

Nanomaterials are incorporated in electrospun CA nanofibers to increase their efficiency in different applications. The incorporation of TiO_2 nanoparticles is hyphosized to improve the properties of the CA/TiO_2 nanofiber composite. Shaukat et al, (2015) synthesised regenerated bacterial cellulose (RBC) nanocomposites with TiO_2 nanoparticles to enhance the bactericidal activity and tissue regeneration properties of BC. The antibacterial activity of the synthesised nanocomposites was tested against *E. coli* by measuring the optical density (OD) and colony forming unit (CFU). The RBC-TiO_2 nanocomposites demonstrated potential bactericidal and biocompatible properties and could be effectively applied in the medical field. Zeng (2010) prepared TiO_2 using the sol-gel method and immobilized it in cellulose matrix for photocatalytic degradation of phenol under weak UV light irradiation. The TiO_2/cellulose composite films revealed good photocatalytic activity.

(b) Polyacrylonitrile

Polyacrylonitrile is a well-known carbon fiber precursor and is also used for activated carbon (Wang & Kumar 2005). It is one of the most commonly studied polymer materials due to its superior properties, which include high mechanical properties, good thermal and chemical stability and possess better processing ability (kharaghani et al., 2018; He et al., 2018). PAN is a semi-

crystalline synthetic polymer obtained through free radical polymerisation of acrylonitrile. The functional groups can become the subject of radical interactions. PAN is a synthetic semicrystalline polymer and has demonstrated superior performance in membrane applications and has also been established to be the best precursor for the production of high performance carbon fibres (Hao et al., 2018). PAN that is electrospun into nanofibers has improved additional characteristic properties which make the nanofibers applicable in different fields.

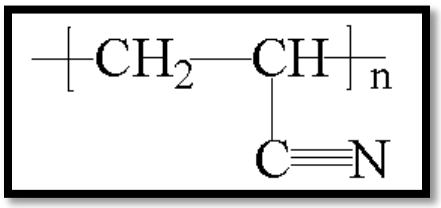

Figure 1.4: Chemical structure of polyacrylonitrile.

Electrospun PAN nanofibers have very high surface area and higher surface to volume ratio attributed to its nanoscale diameter size. Moreover, they are highly porous and this renders the PAN nanofibers useful for filtration application, heavy metal removal from contaminated water, antimicrobial applications and air filtration (Wahaba et al., 2018). Nyamukamba et al., (2016) reported effective degradation of methyl orange using titanium dioxide nanoparticles immobilized on PAN nanofibers. This is mainly because PAN is polar and methyl orange is also polar, therefore, the interaction between the adsorbate and the surface sites of the adsorbent was enhanced. Furthermore, the increased crystallinity of TiO_2 increased the photocatalytic activity of the TiO_2 nanoparticles.

1.2.2. Incorporation of TiO_2 nanoparticles on polymer blended fibers

The incorporation of inorganic nanoparticles into polymer nanofibers improves optical, catalytic, and thermal properties. These properties of polymer nanofibers depend on the type of incorporated nanoparticles, their size, shape, their concentration and interaction with polymer matrix (More et al., 2015). TiO_2 is regarded as a good photocatalyst due to its high catalytic activity, stability against photon corrosion, can be supported on different substrates and its ability to mineralize organic pollutants (Seema et al., 2013). However, TiO_2 has its drawbacks which are associated

with its wide band gap (~3.2eV). Immobilization of TiO_2 nanoparticles on different substates has gained more interest due to its economic advantages (Sookwan et al., 2014; Seema et al., 2013). In addition to improving the photocatalytic and antimicrobial properties of the blended fibers, TiO_2 nanomaterials can make the fibers to be more applicable to a wide range of applications. In this study, TiO_2 nanoparticles will be incorporated in polymer blends of PAN/CA electrospun nanofibers. CA has good characteristics such as thermal stability, chemical resistance, mechanical strength, low toxicity and biodegradability (Wook et al., 2015). However, it is difficult to electrospin CA nanofibers due to its polycationic nature in solution. To overcome this shortcoming of CA, mixing CA with other synthetic polymers such as PAN improves its electrospinning ability. Polyacrylonitrile is one of the most commonly studied polymer materials due to its high mechanical properties, thermal stability, high electrolyte uptake and better processing ability (He et al., 2018). These properties make PAN widely applicable in various fields. A blend of PAN and CA not only has good characteristics of each component, but also has other useful properties such as electrospinnability of the polymer blend. Ocwelwang et al., (2012) synthesised Ag/N-doped TiO_2 nanoparticles via sol-gel method and immobilized them on electrospun chitosan-poly(vinyl-alcohol-co-ethylene) nanofibers to evaluate the photocatalytic and antibacterial properties of the nanofibers. The antimicrobial and photocatalytic activities of the materials were tested against *E.Coli* microorganism and methyl blue dye, respectively. Ag-doped TiO_2 nanoparticles enhanced degradation of methylene blue and was able to trap the photo-generated electrons preventing recombination. Therefore, higher photocatalytic and antimicrobial activities were observed with Ag-doped TiO_2 nanoparticles compared to N-doped titania. Kumar et al., 2018 investigated effective removal of metal ions and cationic dye from water using electrospun carbon nanofibers/TiO_2-PAN hybrid membranes. The electrospun CNFs/TiO_2-PAN hybrid membranes showed an 84% rejection for cationic methylene blue dye, thus this shows potential of hydrophilic electrospun CNFs/ TiO_2-PAN hybrid membrane as filters for heavy-metal ion and dye.

1.3. Electrospinning technique

Several methods have been used for the synthesis of polymer fibers such as chemical vapour deposition, template-assisted synthesis, self-assembly, electrospinning and wet chemical synthesis. Among these methods, electrospinning has gained more interest precisely due to its ability to produce nanofibers with unique properties. It was first discovered in the early 1930's

patented for the first time by Formhals and the work was considered as the first significant study in electrospinning. In 1934, the process and the apparatus for producing continuous fibers through electric charge was described (Moheman et al., 2015). In the mid-1990s, interest increased in the field of nanoscience's and nanotechnology that researchers started to realize the potential of the electrospinning technology. Since then, electrospinning gained more attention due to its capability in spinning a wide variety of polymeric fibers and its consistency in fabricating fibers in the submicron range. Electrospinning produces fibers with nanoscale diameters and these fibers are called nanofibers (Thandavamoorthy et al., 2004). These nanofibers possess favourable characteristics, such as large surface area, high efficiency and high reproducibility. Moreover, electrospinning has been considered as a simple and low-cost approach (Xiaomin et al., 2015).

1.3.1. Electrospinning process

The electrospinning process involves the use of electrostatic forces applied on solutions or melts to produce fibers with diameters ranging from nanometer to micrometer scale. Electrospinning setup consists of three primary components: a high voltage power supply, a syringe with metallic needle and a grounded collector (Yorden et al., 2015). In the usual electrospinning process, a high voltage is applied on the polymer solution, which causes electrostatic charging of the droplet of the polymer. A charged jet of polymer solution is ejected from the tip of the needle when the applied electric field overcomes the surface tension of the polymer droplets (Baji et al., 2010). The interaction between the electric field and the surface tension of the fluid stretches the jet stream, leading to the evaporation of the solvent. This causes the jet stream to be elongated and eventually travels to the grounded collector through spiralling loops forming uniform fibers (Thandavamoorthy et al., 2004; Xiaomin et al., 2015).

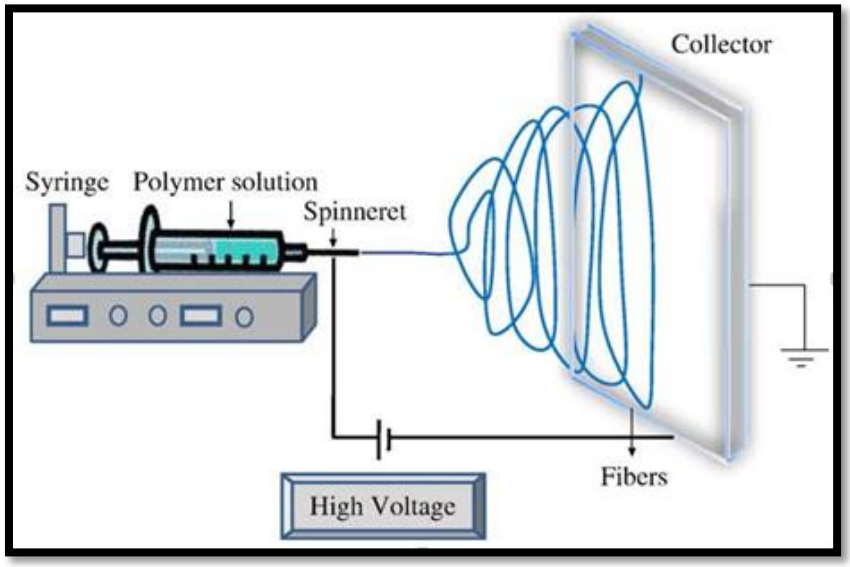

Figure 1.5: Schematic diagram of the typical electrospinning setup (Rafiei et al., 2014).

1.3.2. Factors influencing the electrospinning process

The electrospinning process has various parameters that influences the final fiber features. These parameters are named the solution parameters, process parameters and ambient parameters. The formation of the electrospun nanofibers is influenced by the process parameters such as tip to collector distance, applied electric field and the rate at which the solution flows. The morphology and diameter of the electrospun nanofibers depend on the solution parameters such as viscosity, molecular weight, surface tension and conductivity. Therefore, it is important to control these electrospinning parameters to form uniform nanofibers with desired morphology and diameter.

(a) Effect of concentration

Concentration is one of the significant factors determining the diameter and morphology of the elctrospun nanofibes. The increase in fiber diameter is influenced by the increasing solution concentration. Below certain concentrations, beads and droplets will form instead of fibers due to the solution surface tension. At very high concentrations, fibers are difficult to form due to high viscosity and the inability to control the flow rate of the solution through the capillary resulting in large fiber diameter (Pillary et al., 2013). At lower concentrations, the solution is stretched easily during electrospinning resulting in smaller fiber diameter. High concentrations result in lager diameter size due to the viscosity of the solution being high enough for sufficient entanglement of

the polymer chain. Chowdhury & Stylios (2010) reported the effect of concentration on morphology of electrospun nylon 6 fibres. The results showed that at lower concentration of Nylon 6 solution in formic acid, mostly droplets and a mixture of short fibers with beads were observed. As the concentration was increased from 15 to 20 wt%, the number of beads size decreased and the fiber diameter increased. At 25 wt %, uniform fibers without beads were observed and the fiber diameter gradually increased due to the increase in viscosity. Zhou et al., (2016) investigated the electrospinning of cellulose acetate fibers by varying the solution concentration of 12, 14 and 16 wt%. It was observed from the results that the diameter of CA fibers decreased with decreasing CA mass concentration due to the viscosity of the CA solution decreasing with the decreasing mass concentration.

(b) Effect of voltage

Applied voltage plays a significant role in the fabrication of electrospun nanofibers as it influences the fiber diameter, the shape of the taylor cone at the tip of the needle and the velocity of the polymer jet towards the ground collector. The applied voltage has been reported to have less influence towards the diameter and morphology of the nanofibers, hence, the significance of the applied voltage depends on the concentration of the polymer solution and the distance between the tip of the spinneret and the ground collector. A study by Beachley & Wen 2008 reported a decrease in polycaprolactone fiber length and diameter with increasing voltage, but only a few diameter decreased over all the difference between the 10 kV & 15 kV and 10 kV &20 kV groups. Baker et al., (2018) reported the effect of voltage on polyacrylonitrile electrospun nanofibers and the results showed an increase in fiber diameter as the voltage increased. This increase in fiber diameter with the increasing applied voltage is attributed to the decrease in electrical conductivity and fiber diffusion.

(c) Effect of other process parameters

(i) Distance: The distance from tip of the needle and the ground collector is an important factor that influences the fibers morphology and diameter. This influence depends on the evaporation rate of the solution solvent as it travels to the collector and the deposition time (Heikkila & Harlin 2008). Wet and beaded fibers are produced when the distance from the tip of the needle and the ground collector is small, this is due to the solutions requiring more distance for the solvent to evaporate to produce dry fibers (Haider et al., 2018). As the distance increased, uniform thinner fibers are

produced due to enlargement of the distance between tip of the needle and the ground collector. Tuck et al., (2012) electrospun poly-L-lactide (PLLA) nanofibers by varying the tip-to-collector distance. The results showed poor morphology of the electrospun nanofibers at small distance precisely due to the incomplete evaporation of the solvent by the time the fiber reached the collector. The increase in distance produced fibers with improved alignment compared to shorter distances, this is due to the extensive distance given for the fiber to stretch.

(ii) Flow rate: In electrospinning process, polymer flow rate is a crucial element that not only influences the jet velocity but also the material transfer rate. At lower flow rate, fibers with smaller diameters are produced and this is due to enough time that the solvent gets to evaporate. At high flow rate, the fiber diameter increases and beads may be produced (Zargham et al., 2012). This may be attributed to the incomplete drying of the polymer fiber before reaching the collector. Vashisth et al., (2014) investigated the effect of flow rate on the gellan-PVA nanofibers, the results showed that lower flow rate produced fibers of smaller diameter and as the flow rate increased, the fiber diameter also increased.

(d) Effect of other solution parameters

(i) Solution conductivity: Solution conductivity is one of the crucial factors that affects the diameter of the fiber and the Taylor cone based on the type of polymer, solvents and the presence of ionizable salts. Solution with lower conductivity have less charge carrying capacity to form a Taylor cone as compared to the more conductive solution, hence, this low conductivity hinders the electrospinning process. Increasing the conductivity of the solution increases the charge of the surface of the droplet forming a Taylor cone and also decreases the fiber diameter (Haider et al., 2013; Matabola & Moutloali 2013). Furthermore, the Taylor cone does not form when conductivity is increased beyond a certain value hindering the electrospinning process. The quality of the nanofiber is dependent on the formation of the taylor cone, if the Taylor cone is not formed electrospinning will be hindered due to the surface of the droplet not carry any charge. The charge carrying capacity of the jet is increased by the ions, thereby subjecting it to higher tension with the applied electric field (Matabola & Moutloali 2013). The interaction of the polymer solution with ionic salt could maintain the conductivity of the polymer solution. The loading of salt increases the number of ions in the solution which increase the conductivity and surface charge density resulting in greater stretching and elongation forming thinner diameter fibers (Haider et al., 2018).

Son et al., (2004) reported the effect of adding $AgNO_3$ on morphology and diameter of the electrospun cellulose acetate (CA) nanofibers. The results showed that, with the addition of $AgNO_3$, the fiber diameters were dramatically decreased. The addition of $AgNO_3$ increased the conductivity and the charge density of the CA solution, as a result, stronger elongation forces were imposed on the ejected jets under the electrical field, resulting in substantially straighter shaped and finer CA fibers.

(ii) Surface tension: In the process of electrospinning, surface tension of the solution is one of the important factors that influences the formation of beads, sprayed droplets and fibers. Polymer solution with high surface tension inhibits the electrospinning process due to the capillary instability of the fluid jet and molecules being far apart for effective entanglement to occur (Reneker & Yarin 2008). Tarus et al., (2016) prepared cellulose acetate (CA) and Poly (Vinyl Chloride) (PVC) nanofibers at different concentrations using different solvents mixtures. From the results, beads that were connected by fine strings were observed at lower concentrations and as the concentration was increased, the undesired beads were removed, thus, uniform fibers with an increased diameter were produced. The low solution viscosity possess low viscoelastic force which causes the jet to partially break up under the effect of surface tension and the solvent molecules in the solution being far apart for effective entanglement to occur. Moreover, the formation of beads at lower concentrations and uniform fibers with increasing concentration is due to the change in viscosity of the solution.

1.4. Problem Statement

The issue of contaminated water with microorganisms has become threat to both the physical and social health of living organisms. The non-selective use of antibiotics on bacteria and viruses has led to drug resistance of many bacterial strains making antibiotics less effective. Some antibiotics have serious undesirable side effect which limit their application. Pathogenic bacteria that are mostly found in water such as *Escherichia coli* and *Staphylococcus aureus* causes cutaneous infection, diarrhea and urinary tract infections. Nanotechnology brings greater hope to offering new improved antibacterial agents that are very effective with minimal side effect. Various nanoparticles such as zinc oxide, silver and copper oxide have been used for antimicrobial activity, these nanoparticles have some side effects that can be hazardous to the environment. Among these nanoparticles, TiO_2 has received more attention due to its ability to degrade organic contaminants

and kill microbial cells. Though TiO_2 is efficient it has limitation associated with its wide band gap (3.0-3.3 eV) which only allows 3-5% of visible light. Also, the use of TiO_2 in powder form makes it difficult to filter from aqueous solution after treatment of the polluted water due to the small size of the particles. This means that TiO_2 nanoparticles cannot be reused and may causes water contamination which may be harmful to living organisms. The immobilization of TiO_2 on polymer substrate may solve the problems associated with the band gap to allow use of direct sunlight for photodegradation of organic dyes and enhance the antibacterial properties of the TiO_2 nanoparticles. Incorporation of TiO_2 onto cellulose acetate enhances the antibacterial activity of the composite because CA is a natural organic polymer and blending CA with PAN possess better processing ability and enhances the mechanical strength of the blended composite making it possible for the nanocomposite to be reused.

1.5. Aim and Objectives

1.5.1. Aim

This study aims to fabricate TiO_2 nanoparticles reinforced polymer blended electrospun nanofibers with effective antimicrobial activity against selected microorganisms found in contaminated water and photocatalytic activity for degradation of model organic pollutant in water.

1.5.2. Objectives

The study had the following objectives:

- To synthesise TiO_2 nanoparticles using the sol-gel method.
- Optimization of the electrospinning process for the production of the nanofibers. Parameters to be investigated include polymer solution concentration, spinning voltage, spinning distance and polymer blend ratio.
- Immobilization of various loadings of TiO_2 nanoparticles into the optimised polymer blend ratio using electrospinnig method.
- To test the antimicrobial properties of TiO_2 nanoparticles immobilized on PAN/CA nanofibers against *E. coli*, *S. aureus* and *C. albicans*.
- To evaluate the photocatalytic activity of TiO_2 nanoparticles immobilized on PAN/CA nanofibers using methyl orange (MO) as a model organic pollutant in aqueous medium.

Chapter 2
Research Methodology

2.0. Background

This chapter outlines the experimental procedures for the synthesis of TiO_2 nanoparticles. Sol-gel method was used to synthesise TiO_2 nanoparticles and the calcination temperature was varied in order to control the diameter size, morphology, and distribution of the nanoparticles. Furthermore, the electrospinning technique was used for fabricating the polymer nanofibers and polymer composites. Various parameters such as solution concentration, voltage, blend ratio and loading of TiO_2 nanoparticles onto the polymer blend were varied in order to control diameter size and morphology of the nanofibers.

2.1. Experimental Details

2.1.1. Chemical reagents and apparatus

Titanium tetrachloride ($TiCl_4$) (99%), deionised water, NaOH, Cellulose acetate (30,000 Mn), PAN (Mw =150,000 $g.mol^{-1}$), methanol (99% purity), acetone (99% purity) and N, N-dimethylacetamide (DMAc; Assay: 99%). Three necked round bottom flask, magnetic stirrer, programmable furnace, centrifuges, beakers, vails, magnetic stirrer bars, plastic syringe, stainless-steel needle and aluminium foil. The chemical reagents that were used in this study were supplied by Merck and Sigma-Aldrich South Africa and used without further purification or treatment.

2.1.2. Preparation of TiO_2 nanoparticles using the sol-gel method

The materials used for the synthesis of TiO_2 nanoparticles were 9 M $TiCl_4$ as precursor, distilled water as solvent and NaOH as neutralizer. The TiO_2 nanoparticles were prepared by slowly adding 6 mL of $TiCl_4$ into 200 mL of distilled water in a 250 mL three-neck round bottomed flask immersed in an ice bath (0 ^oC) and stirred vigorously. The flask was removed from the ice bath and was kept in magnetic stirrer to make a homogeneous solution for 45 min at 90 ^oC. The solution was allowed to cool and neutralized to a pH of 8.0 using 10 M NaOH to aid the process of gelation

then heated again for 30 min while stirring. Centrifugation was used to separate the expected white gel from solution. The precipitate was washed repeatedly with deionized water to remove the chloride ions and methanol to prevent agglomeration between precipitates. After a thorough wash the precipitate was filtered and allowed to dry at 110 ºC in an oven overnight. The dried material was crushed into powder using a mortar and pestle and calcined in a programmable furnace at different temperatures of 400, 500 and 600 ºC for 2 hours (Ocwelwang et al., 2012).

2.1.3. Preparation of CA and PAN nanofibers

The preparation of cellulose acetate and PAN solutions was done by dissolving the polymers in separate reaction flasks at different weight percentages in order to find the most suitable solution for electrospining. CA was dissolved in a mixture of N, N-dimethylacetamide (DMAc)/ acetone (1:2 v/v) to prepare 14, 16 and 18 wt% solution for electrospinning. PAN was dissolved in N, N-dimethylacetamide (DMAc) to prepare 10, 12 and 14 wt% solution for electrospinning. The solutions were left overnight under magnetic stirring at room temperature to obtain the desired weight percentages. Separately, the cellulose acetate and PAN solutions were delivered through a 20-ml plastic syringe fitted with a stainless-steel needle of tip-dimensions of 1.20 × 38 mm at a flow rate of 0.040 mm/min. A high-voltage power supply was used to produce the voltages of 20, 22 and 24 kV, and the distance between the nozzle and the collector screen was kept at 15 cm. A stationary metallic roller covered with an aluminium foil was used as a collector for the nanofibers (Matulevicius et al., 2014).

2.1.4. Preparation of PAN/CA polymer blended nanofibers

The PAN/CA polymer blend was prepared by first considering the optimum solutions of the separately electrospun polymer nanofibers out of the three different concentrations of CA and PAN. 16 wt% of CA was blended with 10 wt% of PAN at blend ratios 90:10, 80:20 and 70:30 PAN/CA and CA/PAN. The solutions were left overnight under magnetic stirring at room temperature to obtain well blended polymer solutions. The polymer blended solutions were placed in a 20-ml plastic syringe fitted with a stainless-steel needle of tip-dimensions of 1.20 × 38 mm and electrospun at a voltage of 22 kV with distance between the nozzle and the collector screen

kept at 15 cm. A syringe pump was used to feed the polymer solution into the needle tip at a rate of 0.040 mm/min.

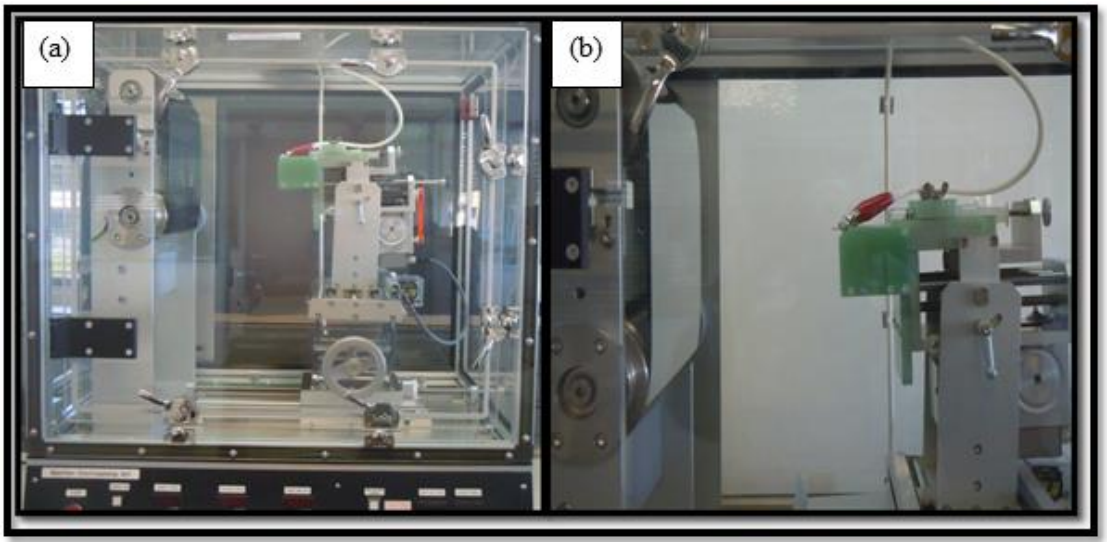

Figure 2.1: Electrospinning system used in the study (a), expansion of the assembly of the needle and collector parts (b).

2.1.5. Incorporation of TiO_2 nanoparticles into PAN/CA polymer blend.

PAN/CA/TiO_2 nanocomposites were prepared by adding 1, 2 and 3 wt% of TiO_2 nanoparticles in the 80/20 polymer blends of PAN/CA solutions. The mixtures were stirred for 5 h. After stirring, the solutions were electrospun and the resultant nanofibers were characterised to determine the newly formed functional groups using FTIR and the XRD was used to determine the presence of TiO_2 nanoparticles. The diameter and morphology of the nanocomposites was characterized using SEM (Chen et al., 2009; Nyamukamba et al., 2016).

2.1.6. Antibacterial tests

Model microorganisms

Staphylococcus aureus (Gram positive bacteria), *Escherichia coli* (Gram negative bacteria) and *Candida albicans* (yeast).

Agar plate method

Antibacterial activity of electrospun pure PAN, pure CA, PAN/CA blended nanofibers, PAN/TiO_2 and PAN/CA-TiO_2 nanofibers was carried out by zone of inhibition assay using the agar plate method against bacterial strain. *E Coli, S. aureus* and *C. albicans* fungi. The bacterial strains culture were grown overnight at 37 °C by adding a single bacterial colony in 100 ml Mueller-hinton (MH) Broth. The overnight culture (0.1 ml) was plated out onto Nutrient Agar plates using the Aseptic technique. The modified membranes were placed on the surface of the inoculated agar plates, and the plates incubated overnight at 37 °C, inverted. Following incubation, the diameters of the zones of inhibition around the membranes were measured. The zone of inhibition is the area around the membranes in which bacterial growth is stopped due to a bacteriostatic effect of the membranes and it measures the inhibitory effect of membranes towards the bacterium (Liu et al., 2015).

2.1.7. Photocatalytic activity

The methyl orange model dye was used for the catalytic degradation studies. An amount of 10 mg of the synthesised TiO_2 nanoparticles and 4x4 cm of nanofibers made from a composite of PAN/TiO_2 & PAN/CA-TiO_2 were added to 50 ml of the latter dye solution (10 ml/L) and stirred for 30 min in the dark to acquire equilibrium. After 30 min of stirring in the dark the solution was stirred continuously under sunlight. After 30 min of stirring in the dark and at 30 min interval, 2 ml of the aliquots were taken and centrifuged at 10000 rpm for 10 min. The degrees of degradations were monitored using Lambda 35 UV–vis spectrometer (Hir et al., 2017).

2.2. Characterization Techniques

This section discusses the analytical techniques that were utilized in this study for the characterization of the nanoparticles, nanofibers and composite nanofibers.

2.2.1. Ultraviolet Visible spectroscopy (UV-vis)

Wavelength range of 200-800 nm will be used to obtain the visible absorption spectra of TiO_2 nanoparticles, using PerkinElmer Lambda 25 UV/VIS spectrophotometer (ELICO-SL-150). The

samples were placed in quarts cuvettes (1 cm path length) using deionised water as a reference solvent.

2.2.2. Photoluminescence spectroscopy (PL)

A PerkinElmer LS 45 was used to measure the photoluminescence of the particles at the excitation wavelength of 320 nm. The samples were placed in glass cuvettes (1 cm path length).

2.2.3. Transmission Electron Microscopy (TEM)

HITACHI JEOL 100S transmission microscope operated at 80 kV was used to analyse the synthesised TiO_2 nanoparticles. The nanoparticles were diluted in deionised water and a drop of the solution was placed on a carbon-coated copper grid. The samples were dried at room temperature prior to analysis.

2.2.4. Scanning Electron Microscopy (SEM)

The morphologies of the fibers were studied using the FE-SEM (Leo Zeiss) scanning electron microscopy operated at 1.00 kV electron potential difference. The fibers were carbon-coated before the analysis.

2.2.5. Energy Dispersive X-ray spectroscopy (EDX)

Energy Dispersive X-Ray Spectroscopy (EDX) is a surface analytical technique used to identify and quantify elemental composition of a material. When determining the nanofiber composites' elemental composition, the SEM (Leo Zeiss) coupled device operated at 1.00 kV electron potential difference was used.

2.2.6. X-ray diffraction (XRD)

Analysis of CA/PAN fibers were studied using wide-angle X-ray scattering (WAXS) using a D8-Advance (Bruker miller Co) apparatus. Cuk α radiation with a wavelength of λ=1.54 Å was used and measurement were taken at high angel 2Θ range of 5-90º with a scan speed of 0.02 q s^{-1}.

2.2.7. Fourier Transform Infrared spectroscopy (FTIR)

FTIR spectroscopy is an analytical technique used to obtain information about an infrared spectrum and absorption or emission of the sample. It measures how well sample absorbs light at each wavelength in order to reveal the presence of certain functional groups in a molecule. Furthermore, the quantitative and qualitative analysis for organic and inorganic samples are provided. In this study, FTIR spectra of the nanomaterials are obtained from using PerkinElmer spectrum 400 FT-IR spectrometer ranging from 450 to 4000 cm^{-1} with resolution of 4 cm^{-1}.

2.2.8. Thermal Gravimetric analysis (TGA)

The thermal stability of the fibers and the composite fibers were analysed by Thermogravimetric Analysis (TGA). The tests were carried out on PerkinElmer STA 6000 simultaneous thermal analyser under nitrogen with a flow rate of 20 ºC/min using about 2-4 mg of sample at a temperature range of 30 ºC to 900 ºC at a heating rate of 10 ºC/min.

Chapter 3
Results and Discussion

3.0. Introduction

This chapter focused on the synthesis and characterization of nanoparticles and nanofibers' result obtained after characterization using different analytical techniques as well as tests for their applications. TiO_2 nanoparticles were characterized by a combination of TEM, XRD, UV Visible & photoluminescence spectroscopy and incorporated into the polymer blended fibers by varying their percentages. The polymer fibers together with the blends were prepared using electrospinning technique and characterized by a combination of UV Visible spectroscopy, TGA, XRD, SEM and EDX. Their applications included both antibacterial activity against selected species and photocatalytic activity using the selected organic dye. The conditions of synthesis were optimised such as concentration of the polymers, nanoparticles incorporated into polymers, voltages applied in both fibers and blended fibers. The optimal conditions were selected for further exploration in the optimisation process until the best combination of concentration, voltage and polymer percentage are selected for the antibacterial and photocatalytic degradation tests.

3.1. TiO_2 nanoparticles

The nanoparticles were prepared using the sol-gel method as described below in Figure 3.1. The titanium tetrachloride solution was added dropwise into distilled water placed in a three neck round bottom flask immersed in an ice bath with vigorous starring to form the oxide. After the removal of the solution from the ice bath, the solution was stirred for 45 min at 90 ºC and the colour of the solution turned white. The TiO_2 nanoparticles synthesised at different calcination temperatures of 400, 500 and 600 ºC were characterised using the UV-vis, FTIR, PL spectral, TEM and XRD techniques.

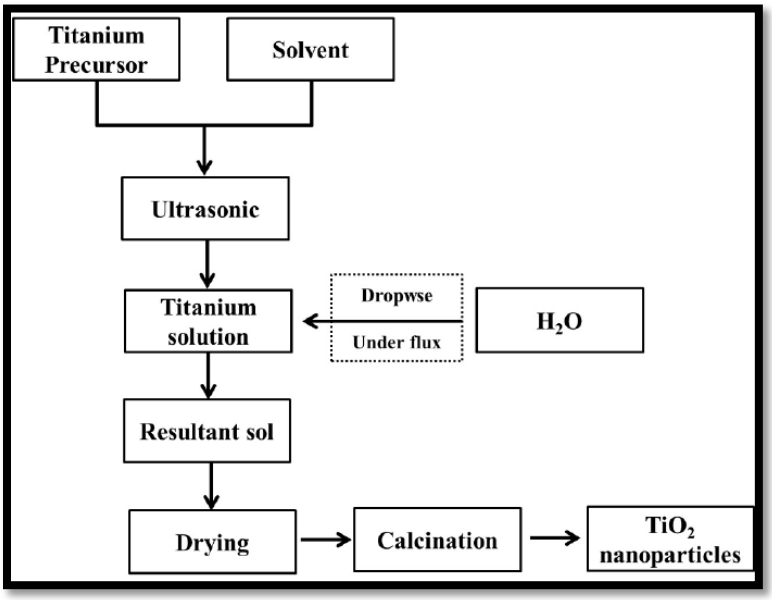

Figure 3.1: Schamatic diagram of the sol-gel process.

3.1.1. Optical properties of the nanoparticles

Titanium dioxide nanoparticles were prepared using the sol-gel method. The sol-gel method increased the possibility of obtaining ultrafine powders which have an extremely large specific surface area. The effect of calcination temperature was investigated to check its influence on the formation of the nanoparticles.

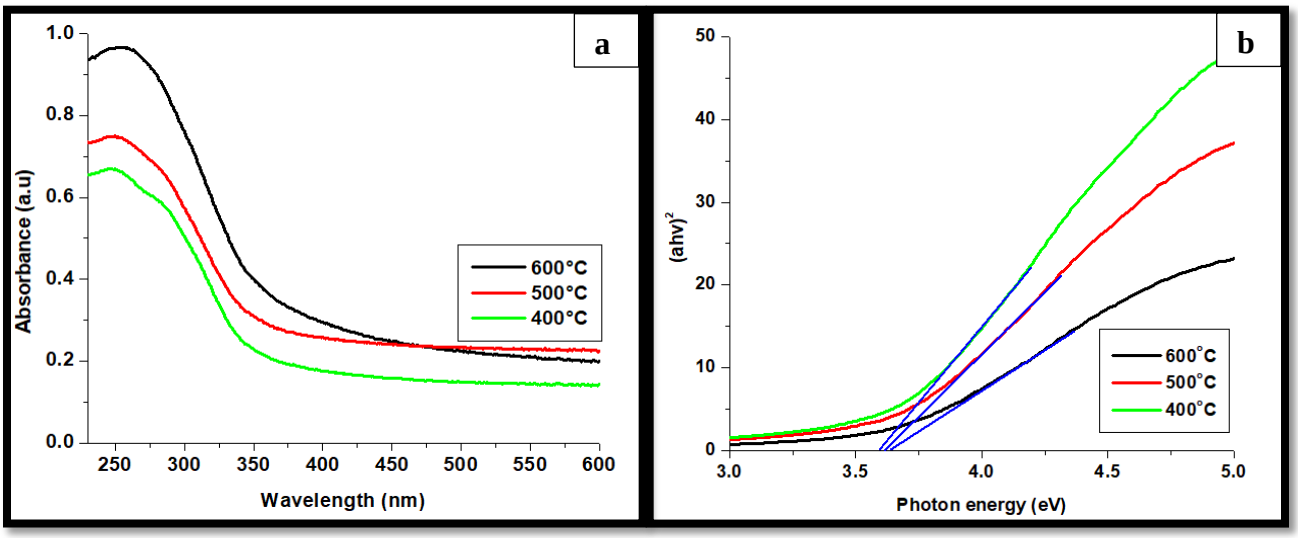

Figure 3.2: (a) Absorption spectra of TiO_2 nanoparticles prepared at different calcination temperatures, 400 ºC, 500 ºC and 600 ºC, (b) Tauc plot.

Calcination temperature is one of the major factors influencing the structural and optical properties of the TiO_2 nanoparticles.

The band gap energy (E_g) of the synthesised TiO_2 nanoparticles was obtained using the equation:

$$E_g=\frac{1240}{\lambda} ev, \qquad \text{(Hayle \& Gonfa 2014)}$$

Where E_g is the band gap electron volt (eV) and λ is the wavelenghth of the absorption edges in the spectrum in nanometer (nm) (Hayle & Gonfa 2014).

Figure 3.2 shows the absorption spectra for the synthesised TiO_2 nanoparticles prepared at different calcination temperatures (400 , 500 and 600 ºC). The variation of the calcination temperature has an effect on the adsorption edges of the particles. Figure 3.2 (a) showed an increase in the absorption edges as the calcination temperature was increased from 400 , 500 and 600 ºC with the adsorption edges of 322, 324 and 335 nm, respectively, showing blue shift from the bulk adsorption edge of 388 nm. The synthesised TiO_2 nanomaterials band gap energy (3.85, 3.83 and 3.70 eV) are larger than the value of 3.2 eV for the bulk TiO_2 nanomaterials. The decrease of the band gap with increasing calcination temperature is due to the increasing nanoparticle size and crystallinity improvent according to the XRD and TEM (Keiteb, 2016). The band gap values confirms the crystallite size of the nanoparticles to which larger bang gap have small crystallite size and smaller band gap have large crystallite size (Hayle & Gonfa 2014). When the particle size increases, the number of atoms that form the particle also increases causing the valence and conduction electons to be more attractive to the ion core of the particle resulting in a decreased band gap on the particle (Keiteb, 2016). The absorption edge of the calcined nanoparticles show a shift to higher energy (blue shift) with a decresed size of the particles as compared to the bulk material.

The Tauc's method was used to calculate the optical band gap of TiO_2 nanoparticles. The tauc plot gives good approximation of the indirect band gap energy of the nanoparticles. The plot of $(ahv)^n$ against hv reveals a linear region just above the optical absorption edge, where n=2 is used for direct allowed transition, n=1/2 for indirect allowed transition, and hv is the photon energy (eV) (Wang et al., 2011; Reddy et al., 2002). Figure 3.2(b) shows the tauc plot for band gap calculations. The blue shift in the absorbance spectra of TiO_2 calcined at 400, 500 and 600 ºC are shown and absorbance edge corresponds to 344, 342 and 341 nm having band gap 3.60, 3.62 and 3.64 eV,

respectively. Figure 3.3 shows the photoluminescence (PL) spectra of TiO_2 nanoparticles calcined at various temperatures of 400 , 500 and 600 ºC with excitation wavelength of 320 nm. Two broad emission peaks appear at 383 nm and 408 nm, which are equivalent to 3.24 eV and 3.04 eV, respectively, showing the red shift from the excitation peak.

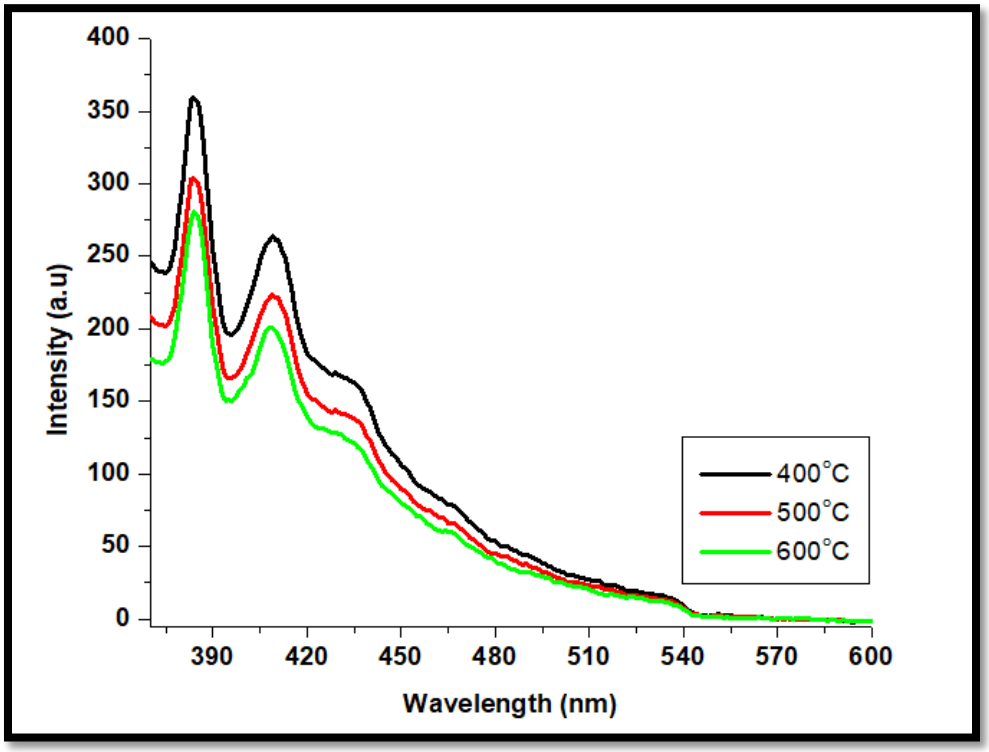

Figure 3.3: PL spectra of TiO_2 nanoparticles prepared at different calcination temperatures of 400 ºC, 500 ºC and 600 ºC.

The difference in the broad PL spectra is due to the various calcination temperatures illustrating the mixed phase structure, surface microstructure and sizes of the TiO_2 nanoparticles. The split of spectrum into two humps is due to the multiple energy levels of mixed phase (anatase and rutile) existing in all the samples calcined at various temperatures. The band edge emission at 383nm can be attributed to the recombination of exciton for all samples. The sample calcined at 400ºC shows high emission intensity than the ones calcined at 500 and 600 ºC due to the self trapped excitons recombination which is a combined effect of defect centres generated from oxygen valences and particle size (Mathpal et al., 2013). With increasing calcination temperature, there is a significant decrease in the excitonic PL intensity of TiO_2 which may be due to the increase in particle size,

high crystallinity and destroyed surface microstructure (Zhou et al., 2008; Chen et al., 2013). Furthermore, the PL spectra revealed three small peaks at wavelength range from 435 to 538 nm which are attributed to excitonic PL mainly resulting from surface oxygen valences of TiO_2 nanoparticles. The PL peaks at 435 and 468 nm are attributed to band edge free excitons. The sample calcined at 600 ºC has the lowest PL intensity due to the increased particle size and better crystallization. The lowest PL intensity indicates that the photogenerated holes and electrons have the lowest recombination rate in the sample. According to literature, it is known that the PL intensity is related to the surface defects of the materials. The decrease in PL intensity can illustrate the decrease in the surface state.

3.1.2. Morphological properties of the nanoparticles

Figure 3.4 shows the TEM images and the size distribution histograms of TiO_2 nanoparticles prepared at different calcination temperatures. TiO_2 nanoparticles appear to have spherical shapes with different average particle sizes of 9.1, 12.2 and 14.0 nm at calcination temperatures of 400, 500 and 600 ºC, respectively. The particles are distributed with less agglomeration and this is due to the temperature effect. TiO_2 nanoparticles calcined at 400 ºC exhibited uniform morphology with particle size of less than 18 nm. As the calcination temperature was further increased from 500 to 600 ºC, the average particle sizes of TiO_2 nanoparticles increased and found to be in the range of 8-24 nm as shown in Figure 3.4 The results showed that the particle size of the nanoparticles increased with an increasing calcination temperatures. This may be due to the interaction of many adjoining particles resulting in more spherical large particle sizes by melting their surfaces. Calcination of TiO_2 nanoparticles enhanced the structural and morphological features especially the crystallinity.

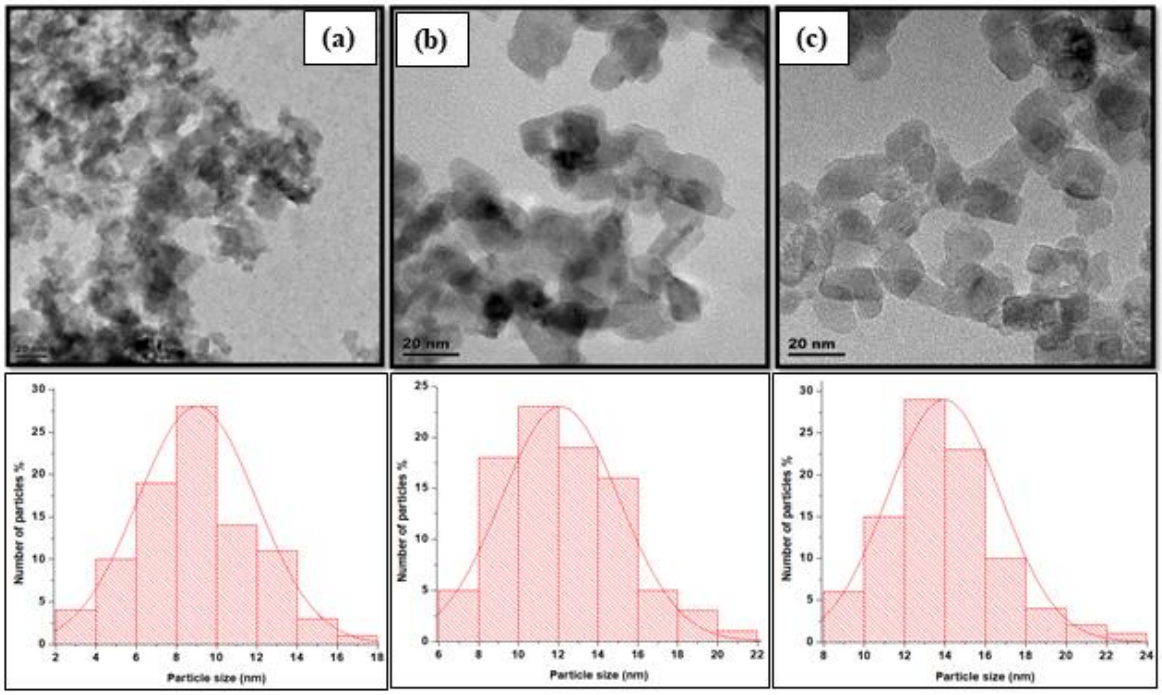

Figure 3.4: TEM image of TiO_2 nanoparticles prepared at different calcination temperatures and the size distribution histogram for samples calcined at (a) 400 ºC, (b) 500 ºC and (c) 600 ºC, respectively.

Calcination, as a process employing temperature, can demonstrate the dependence of the phase transition of titanium dioxide especially for the rutile and anatase phases. Figure 3.5 shows the XRD patterns of TiO_2 nanoparticles calcined at different temperatures of 400, 500 and 600 ºC. The XRD patterns showed sharp and narrow diffraction peaks which indicated the formation of crystalline TiO_2 nanoparticles. It was observed that, as the calcination temperature increased from 400 to 500 ºC, the intensity of both anatase and rutile peaks gradually increased and the removal of some small peaks at lower calcination temperature was observed. Furthermore, as the calcination temperature was increased to 600 ºC, both the anatase and rutile phase became narrower, which indicated the increase of crystallite size, as supported by the TEM images, which is due to the increasing particle size of the TiO_2 nanoparticles. The highest peak at 2Ɵ at 25.5º corresponding to crystal plane (101) of anatase became thinner and the relative intensity was increased with the increasing calcination temperature. The narrow sharp peak signifies that the crystalline phase of anatase was formed and an increasing particle size. As it can be observed from

Figure 3.5, the XRD peaks in the angle range of $20° \leq 2\theta \leq 80°$ determined that from all the three spectra, strong diffraction peaks representing the anatase phase are observed at 2Θ values of 25.5º, 38.2º, 48.1º and 62.44º, corresponding to the crystal planes of (101), (103), (200), and (105), respectively. This shows that the anatase is the dominant phase and this is beneficial since anatase is reported to be more photocatalytically active. Rutile phase was also identified at 2θ values of 27.5º, 41.2º and 56.5º corresponding to the crystal planes of (110), (200) and (211), respectively.

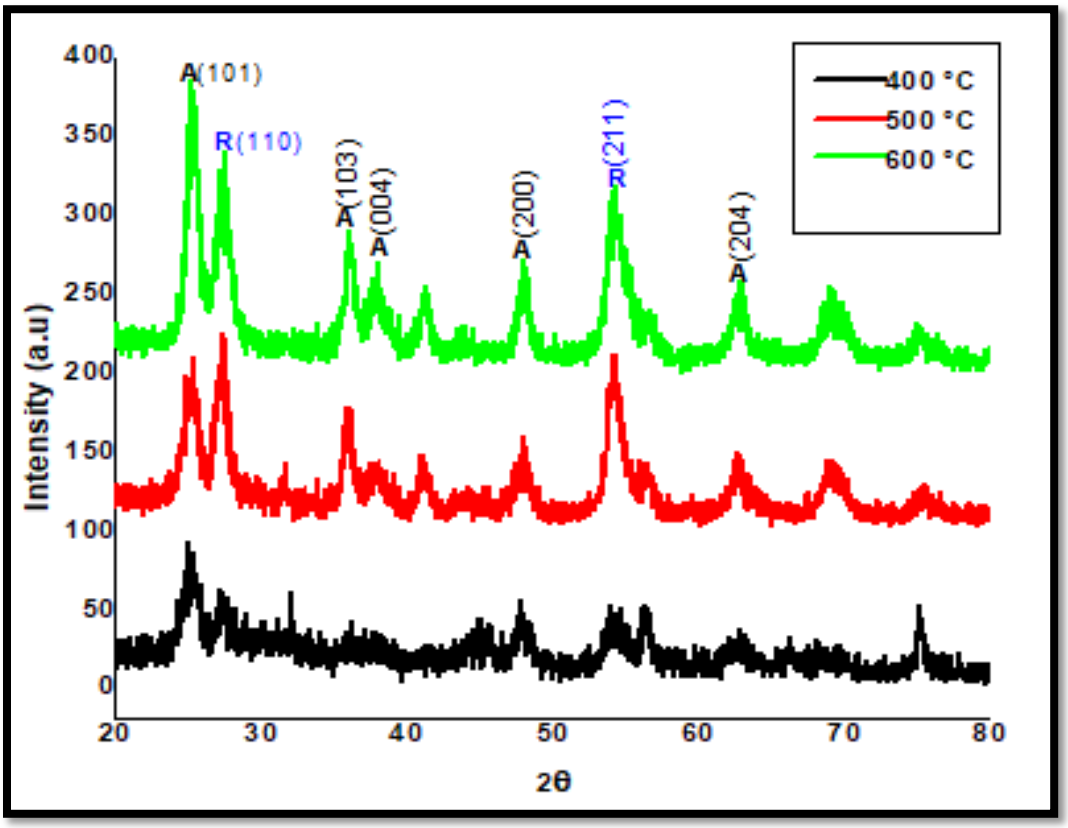

Figure 3.5: XRD patterns of TiO_2 nanoparticles prepared at different calcination temperatures of 400 ºC, 500 ºC and 600 ºC.

3.1.3. FTIR spectral analysis of nanoparticles

FTIR spectra of TiO_2 nanoparticles calcined at different temperatures are shown in Figure 3.6. The peak in the region from 500-900 cm^{-1} is attributed to Ti-O stretching and Ti-O-Ti bridging stretching modes, due to the formation of TiO_2 nanoparticles. The sharp and broad peaks observed

in all three spectra at 1690 cm^{-1} and 3400 cm^{-1} correspond to the O-H bending and stretching modes, respectively, indicating adsorbed water molecules in the nanoparticles. The peak at 2954 cm^{-1} correspond to C-H stretching, which may be due to the use of methanol when washing during the preparation of TiO_2 nanoparticles. As the calcination temperature increased, the surface absorbance water and hydroxyl group decreased slightly. This is due to the removal of a large portion of adsorbed water from TiO_2 and decrease of specific surface area and pore volume, which causes the reduction of the adsorbed water. The adsorbed OH^- ions on the surface of the sample play an important role in photocatalysis by interacting with the photogenerated holes, which improves the charge transfer and hinder the recombination of electron-hole pairs (Dong et al., 2009).

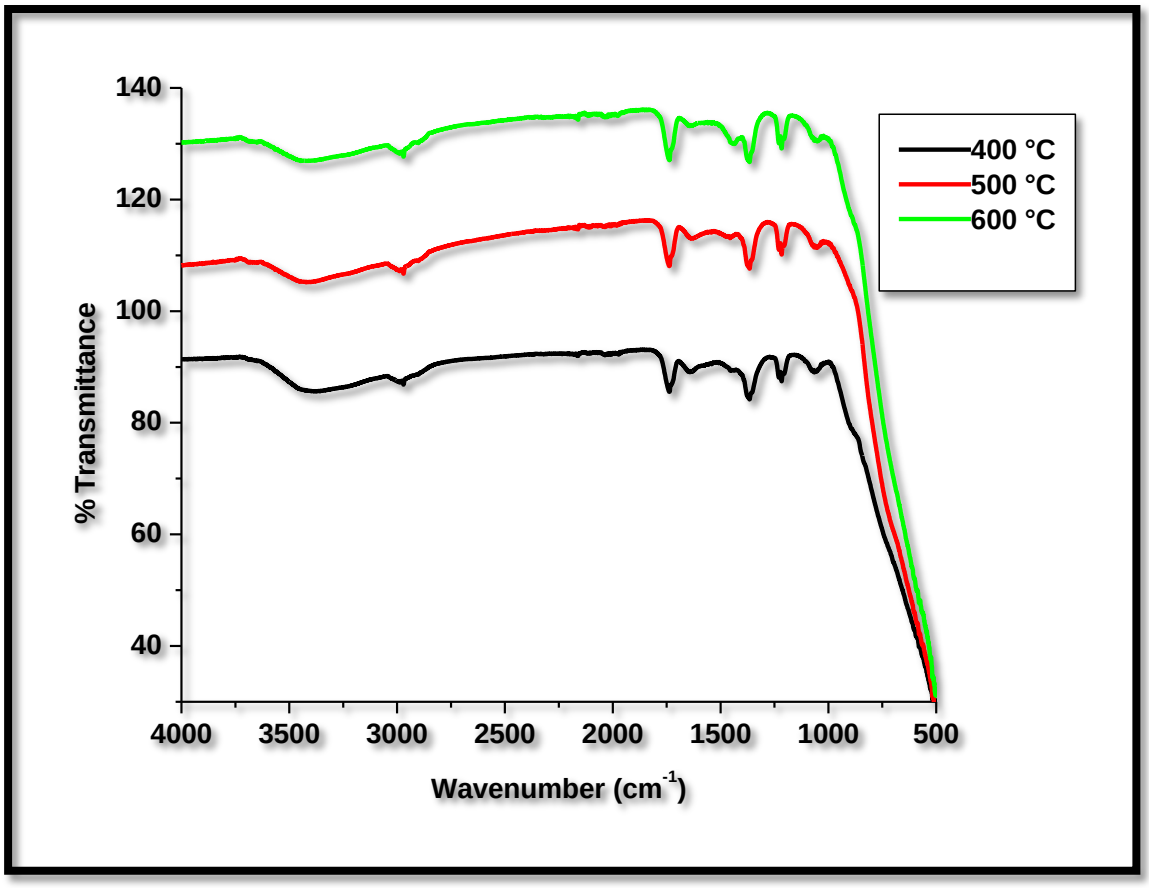

Figure 3.6: FTIR spectra of TiO_2 nanoparticles prepared at different calcination temperatures of 400 ºC, 500 ºC and 600 ºC.

3.2. Electrospun polymer nanofibers

The electrospinning process involves the controlling of different parameters that influence the formation of the polymer nanofibers which exhibit several properties that make them favorable for many applications. Parameters includes the applied electric field, flow rate and tip-to-collector distance. Electrospinning parameters affect the morphology and diameter of the electrospun nanofibers, therefore, by properly controlling these parameters, polymer nanofibers of desired morphology and structure will be acquired. The influence of some of these parameters was studied and is presented in subsections i.e., by varying the polymer concentration, applied voltage and the incorporation of TiO_2 nanoparticles. Addition of the TiO_2 nanoparticles was effective only under conditions of 16 wt% CA and 10 wt% PAN concentration with voltage of 22 kV and spinning distance of 15 cm, respectively. From the XRD results, it was concluded that the best suitable TiO_2 nanoparticles to be incorporated onto CA, PAN and PAN/CA blended polymers were the nanoparticles calcined at 500 ºC for two hours for the fabrication of high crystalline nanomaterials. When comparining the nanoparticles calcined at 500 ºC with the other nanoparticles, samples calcined at 500 ºC are completely crystallized as compared to the ones calcined at 400 ºC and have smaller particle size and large surface area as compared to the ones calcined at 600 ºC. Nanoparticles calcined at 500 ºC have different phases of both anatase and rutile on the same semiconductor which improves its antibacterial and photocatalytic performance. Moreover, nanoparticles calcined at 500 ºC have the advantage of reducing the recombination effect to enhance the photocatalytic performance due to anatase being the most dominant phase. In this section, results from the characterization techniques such as SEM, EDX, XRD, FTIR spectroscopy and TGA are discussed.

3.2.1. Effect of concentration on polymer (CA and PAN) nanofibers.

It has been shown that the solution concentration in electrospinning has significant effect on the morphology and size of the nanofiber. Solution's surface tension and viscosity are most significant in determining the range of concentrations from which continuous fibers can be obtained in electrospinning. At low concentrations, droplets will form instead of fibers before reaching the collector due to the surface tension. At high concentrations, fibers cannot be formed due to an inability to control and maintain the flow rate through the capillary tip. Furthermore, formation of

beads or fibers mostly depends on the viscoelasticity of the solution, charge density carried by the jet and the surface tension of the solution. Figure 3.7 shows the SEM micrographs of fibers electrospun at different PAN concentrations (10, 12 and 14 wt%) with a voltage of 22 kV and a distance of 15 cm. It was observed that at concentrations below 10 wt%, droplets were formed due to lower concentration and higher surface tension. At concentrations higher than 14 wt%, it became difficult to electrospin fibers due to the higher viscosity of the solution. As the concentration was increased to 10 wt%, uniform fibers were obtained with an average diameter of 228 nm and consistent fibrous morphology. Upon the increase of the polymer concentration from 12 to 14 wt%, the fiber diameter also increased consistently from 284 to 560 nm. At lower concentrations, smaller diameter fibers were obtained due to the easy stretching of the solution during electrospinning and nanofibers with larger diameters obtained at higher concentractions were attributed to the high viscosity of the solution that lowered the bending instability of the jet.

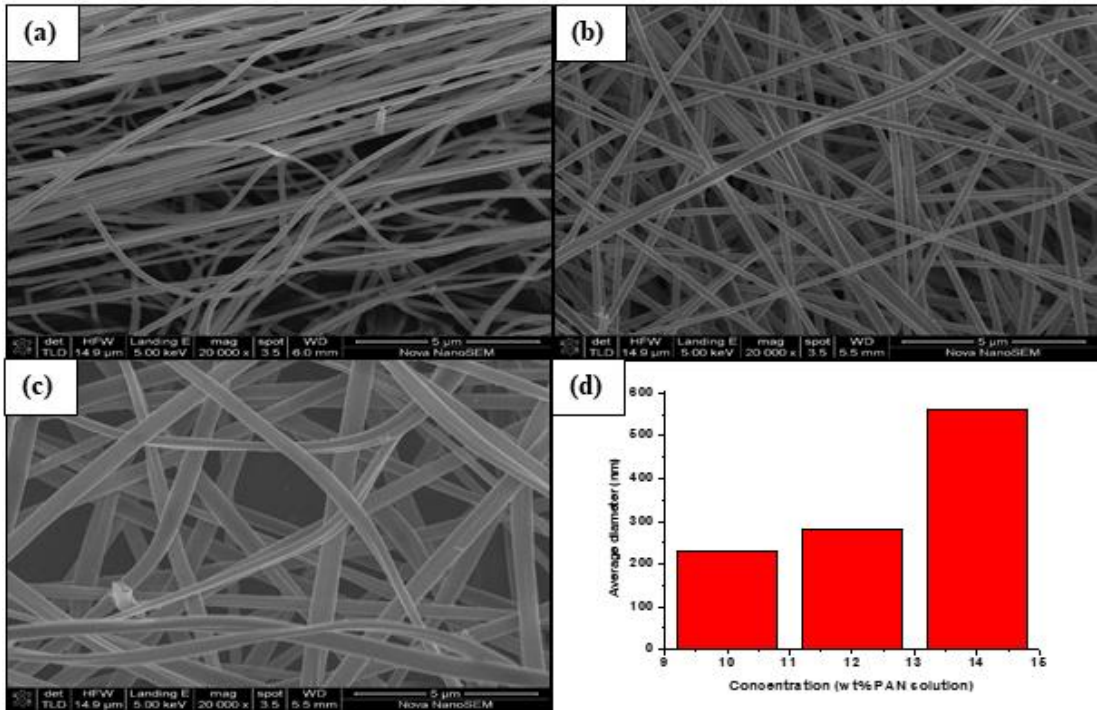

Figure 3.7: SEM images and average fiber diameter distribution (d) of PAN nanofibers at different polymer concentrations 10 wt% (a), 12 wt% (b) and 14 wt% (c).

Figure 3.8 shows the SEM images of fibers electrospun at different CA concentrations (14, 16 and 18 wt%) with a voltage of 24 kV and a distance of 15 cm. At concentrations below 14 wt%, droplets were formed indicating the capillary breakup due to higher surface tension. Electrospinning from

solutions with concentrations higher than 18 wt% was prohibited as a result of high viscosity. At high concentration, larger diameter fibers are obtained due to the viscosity of the solution that was high enough to lower the bending instability of the jet. As the concentration further increased, it became difficult for the highly viscous solution to force through the syringe needle making the control of the solution flow rate to the tip unstable. At 14 wt%, a mixture of beads and fibers were obtained with an average fiber diameter of 173 nm. As the concentration was further increased between 16 and 18 wt%, the fiber morphology changed from beaded fibers to a more consistent fibrous morphology with an average diameter of 338 nm. Surface tension is the dominant influence of the formation of beads at 14 wt% and the morphology change to well aligned fibers at 16 and 18 wt% is due to stability of the electrospinning jet and the sufficient entanglement of the polymer chains.

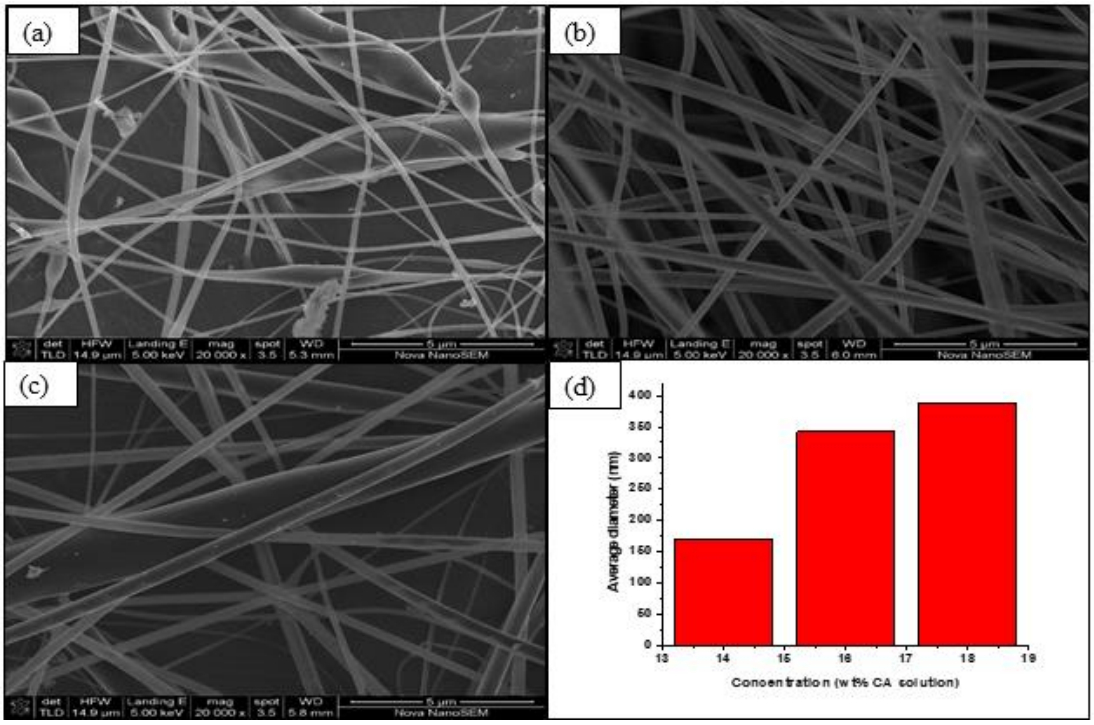

Figure 3.8: SEM images and average fiber diameter distribution (d) of CA nanofibers at different polymer concentrations 14 wt% (a), 16 wt% (b) and 18 wt% (c).

3.2.2. Effect of applied voltage on polymer (CA and PAN) nanofibers.

Applied voltage imposed on polymer solution is one of the essential parameters in the electrospinning process for producing nanofibers. The variation of applied voltage influences the morphologies of the resulting fibers, but need to be considered together with other parameters, particularly the concentration, flow rate and the gap distance. Furthermore, the change in applied voltage affects the shape of the surface at which the Taylor cone and fiber jets formed at the tip of the spinneret and the velocity of the jet. The influence of applied voltage is polymer-dependent, however, no significant effect of the applied voltage or a linear increase in fiber diameter with the applied voltage has been reported by other researchers. Other researchers have reported that, upon an increase in the applied voltage, irregular morphology and larger fiber diameters were observed.

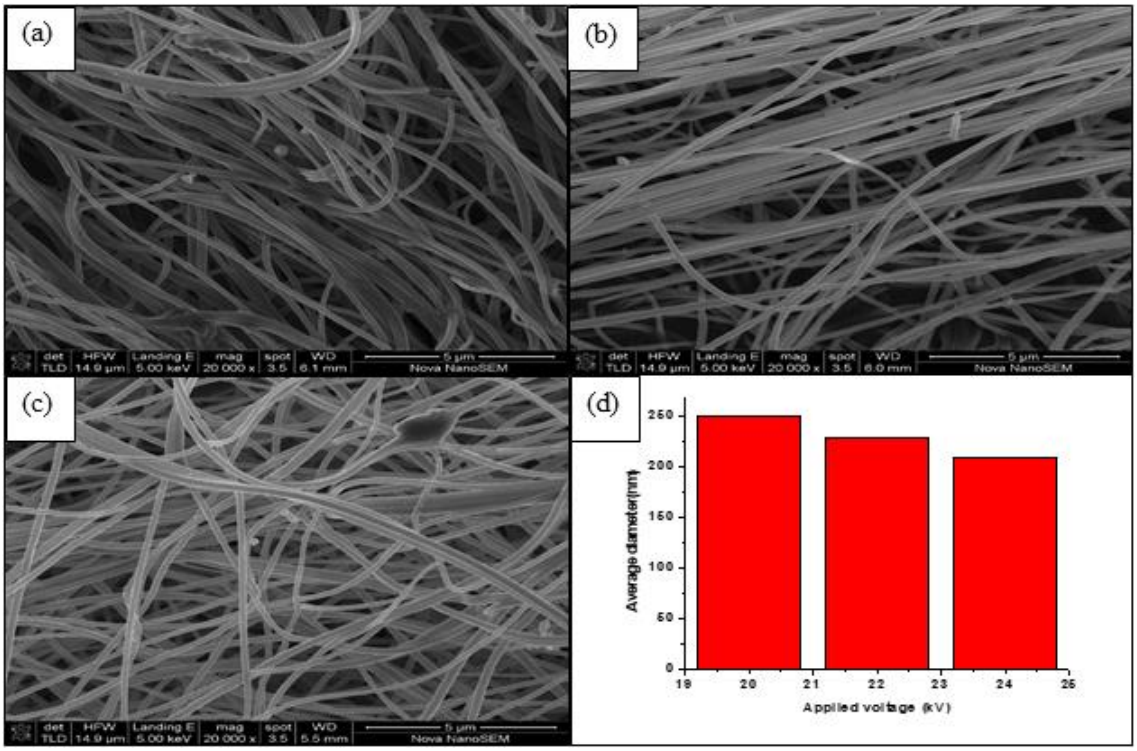

Figure 3.9: SEM images and average fiber diameter distribution (d) of 10 wt% PAN nanofibers electrospun at 15 cm distance and different voltages 20 kV (a), 22 kV (b) and 24 kV (c).

Figure 3.9 shows the SEM images and average fiber distribution of PAN nanofibers at different voltages, with a PAN concentration of 10 wt% and distance of 15 cm. The increase in applied voltage had effect on the morphology. At 22 kV, well aligned fibers were observed and as the

voltage was further increased to 24 kV, the fibers morphology changed to flat ribbon structure. Upon increasing voltage from 20 to 22 kV then 24 kV, the fiber diameter decreased gradually from 248 to 232 nm and then to 220 nm, which suggested that increased voltage caused the solution to be removed from the needle tip quicker than it was supplied. The droplet at the needle tip disappeared completely as the applied voltage increased to 22 and 24 kV, which explains further the decrease in the nanofiber diameter. The increased applied voltage changed the shape of the jet initiating point, hence, this had an effect on the changed morphology of the PAN nanofibers from curled to well aligned nanofibers. A higher applied voltage combined with more concentrated solutions and an increased spinning distance allows greater stretching of the polymer solution due to the viscosity of the solution as well as a strong electric field, resulting in a reduced fiber diameter.

The increased applied voltage had no effect on the morphology and the diameter of the CA nanofibers beadless and uniform fibers were observed at different applied voltages (Figure 3.10). The same diameters of 338 and 337 nm were observed at 20, 22 and 24 kV, respectively. This may be due to the increased charge density on the surface of the jet, polymer jet velocity and polymer strand elongation force making the jet stable. Furthermore, increasing the applied voltage with 2 kV had no effect in forming several jets that produce fibers with fiber diameter less or more than 338 nm. Small voltage gaps of 2 kV were used because at voltage higher than 24 kV, the jet travels fast from the edge of the tip with no visible Taylor cone and this results in formation of fibers mixed with beads. The influence of the applied voltage is dependent upon the type and molecular weight of the polymer.

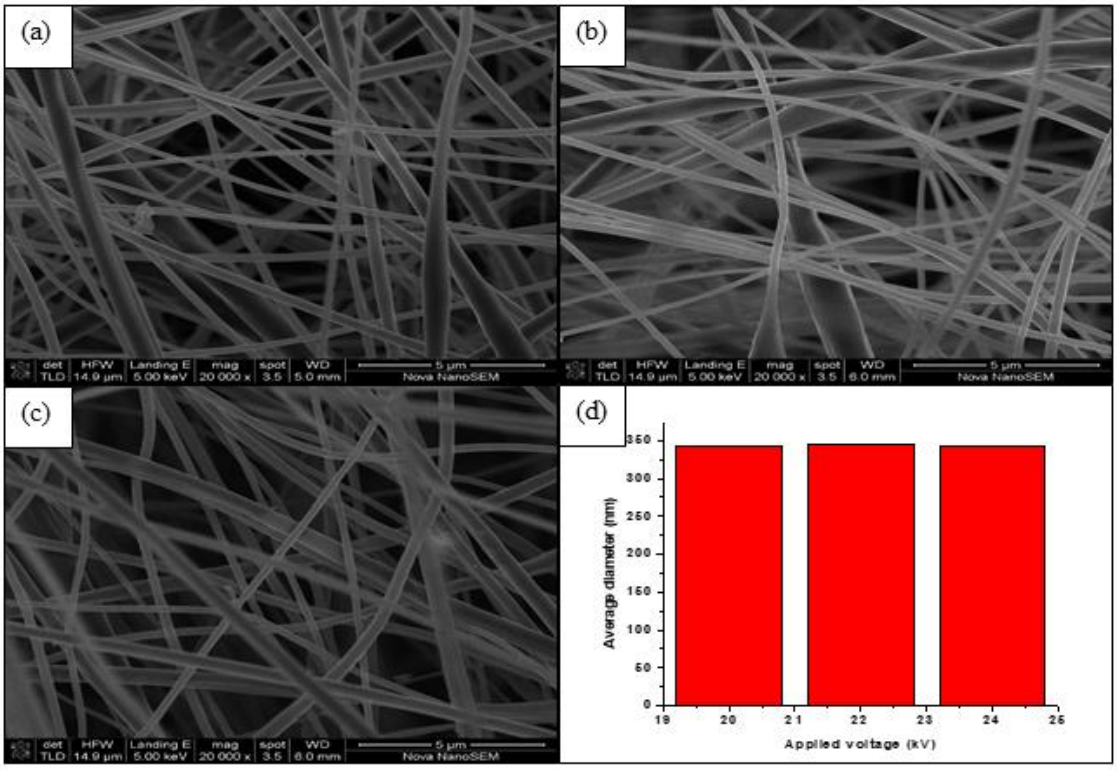

Figure 3.10: SEM images and average fiber diameter distribution (d) of 16 wt% CA nanofibers electrospun at 15 cm distance and different voltages 20 kV (a), 22 kV (b) and 24 kV (c).

3.2.3. Effect of nanoparticles loading on the PAN and CA nanofibers.

There are various factors that influence the fabrication of desired fiber morphology and size such as the viscoelasticity of the solution, charge density carried by the jet and the surface tension of the solution. These factors can be influenced by additives added into the polymer solution. For the incorporation of nanoparticles into polymer fibers, nanoparticles prepared at 500 ºC calcination temperature were used due to their mixed anatase/rutile phases and spherical shape. Figure 3.11 shows the effect of TiO_2 nanoparticles loading of 1, 2 and 3 wt % on the morphology and diameter of the electrospun PAN nanofibers. It was observed that the diameter of pure PAN nanofiber (228 nm) was thicker than that of PAN-TiO_2 composite fibers loaded with 1 and 2wt % TiO_2. The results indicated that the addition of the nanoparticles led to a significant decrease in the fiber diameter. This could be due to the increased electrical conductivity which led to increased surface charge of the polymer jet, and thus, stronger elongation forces were imposed to the jet, resulting in more uniform fibers with a thinner diameter distribution.

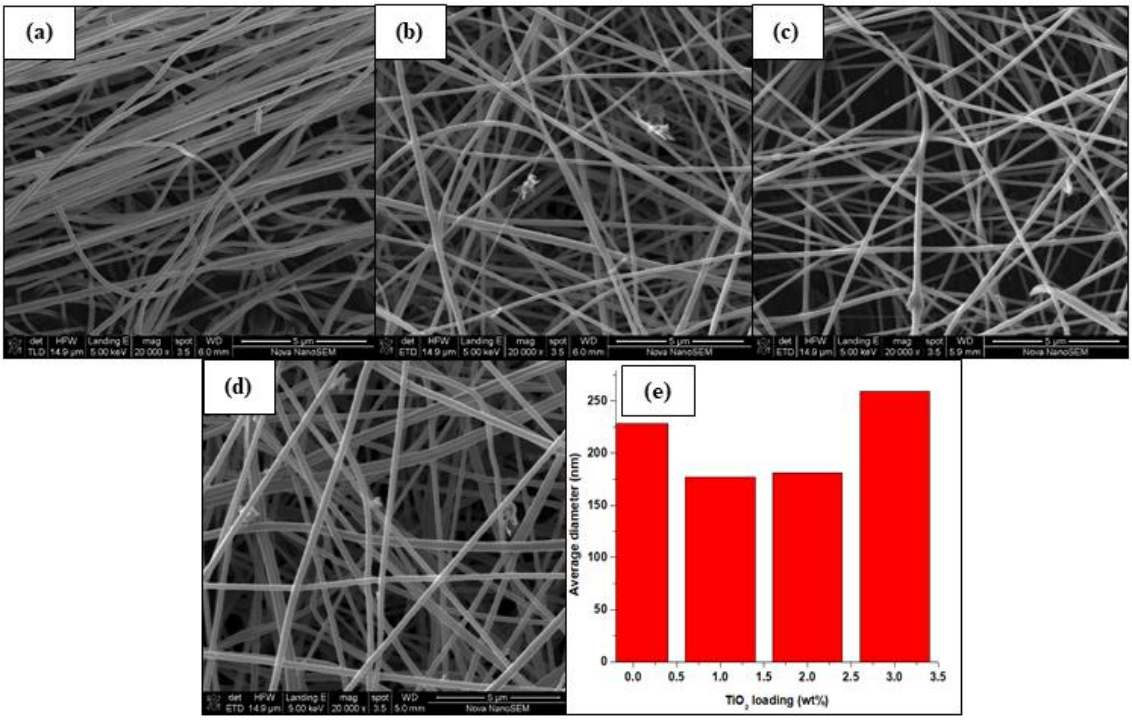

Figure 3.11: SEM images and average fiber diameter distribution (e) of 10 wt% PAN and different loading of TiO_2 nanoparticles 10 wt% PAN (a), 1wt% (b), 2wt% (c) and 3wt% (d) electrospun at 15 cm distance and 22 kV voltage.

Therefore, incorporating TiO_2 nanoparticles into PAN solution enhances the conductivity of the solution to be electrospun and as a result of this improved conductivity, the produced fibers became thinner compared with fibers produced from PAN solution. As the concentration of the TiO_2 nanoparticles was further increased to 3 wt%, the fiber morphology improved while the diameter slightly increased to 259 nm which is greater than that of pure PAN. This could be attributed to the chemical reduction process not taking place due to the increase in solution viscosity, because a high and optimum concentration of polymer was used in combination with nanoparticle addition.

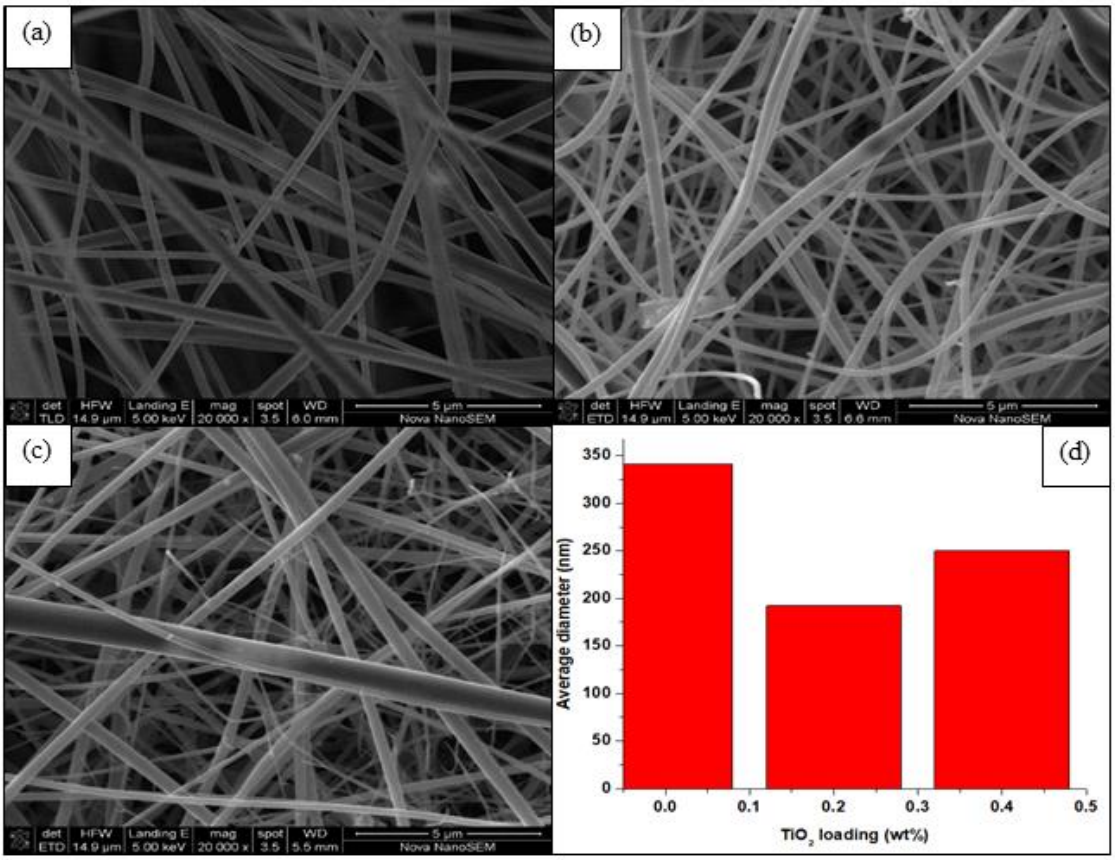

Figure 3.12: SEM images and fiber diameter distribution (d) of 16 wt% CA and different loading of TiO_2 nanoparticles 16 wt% CA (a), 0.2 wt% (b) and 0.4 wt% (c) electrospun at 15 cm distance and 22 kV voltage.

Figure 3.12 shows the effect of TiO_2 nanoparticles loadings from 0.2 to 0.4 wt% on the morphology and diameter of the electrospun CA nanofibers. It is observed that the fiber diameter of pure CA is 338 nm whereas the addition of 0.2 and 0.4wt % nanoparticles improved fiber morphology with a decreased average diameter of 192 and 250 nm, respectively. This decrease in fiber diameter with the addition of nanoparticles is attributed to the conductivity and charge density increase, resulting in greater stretching and elongation of the jet, thereby, causing a reduction in the fibers diameter.

3.2.4. Effect of blending ratio of PAN and CA.

Blending of PAN and CA polymer fibers involves the intereaction between the nitrile group of PAN and CA hydroxyl group. CA has a number of carbon atoms linked with the hydroxyl group, and the redox reaction between solvent ions and hydroxyl group on the surface of CA powder results in the formation of radicals on these carbon atoms. Therefore, when PAN is added, the generated radicals were transferred from CA to the double bonds carbon in PAN monomer for proper blending of the two polymers (Chen et al., 2009). For the blending of PAN and CA polymer fibers, 10 wt% PAN solution was mixed with 16 wt% CA solution at various weight ratios (PAN/CA): 10/90, 20/80, 30/70 90/10, 80/20 and 70/30. Solutions of 10 wt% PAN and 16 wt% CA were used due to their optimum concentration that allows easy stretching of the polymer blend solution during electrospinning to produce smaller uniform nanofibers with large surface area. \Figure 3.13 shows the effect of blend ratios on the morphology an diameter of the resultant fibers. The results were obtained by electrospinning the PAN/CA blend solutions with the voltage of 22 kV at a spinning distance of 15 cm. From the SEM images, it was observed that PAN/CA blends with more amount of CA (10/90, 20/80 and 30/70 PAN/CA) have a combination of beads and thinner fibers. The volume of the CA polymer nanofibers is less than of the beaded formation, this could be due to the viscoelasticity of the polymer blend solution, the charge density carried by the jet, the high surface tension of the solution and the lower polymer molecules for effective chains entanglement to occur. As the amount of CA increased, larger beads with smaller fiber diameters were formed, which shows that CA is not easily controlled despite the changing ratio of blending with PAN. The blends that are PAN rich (90/10, 80/20 and 70/30 PAN/CA) produced uniform fibers without beads with an increasing average diameter of 378 , 538 and 675 nm. The increased amount of CA solution added into the PAN solution led to an increased fiber diameter. The increased fiber diameter is due to the increased viscosity of the PAN/CA blend.

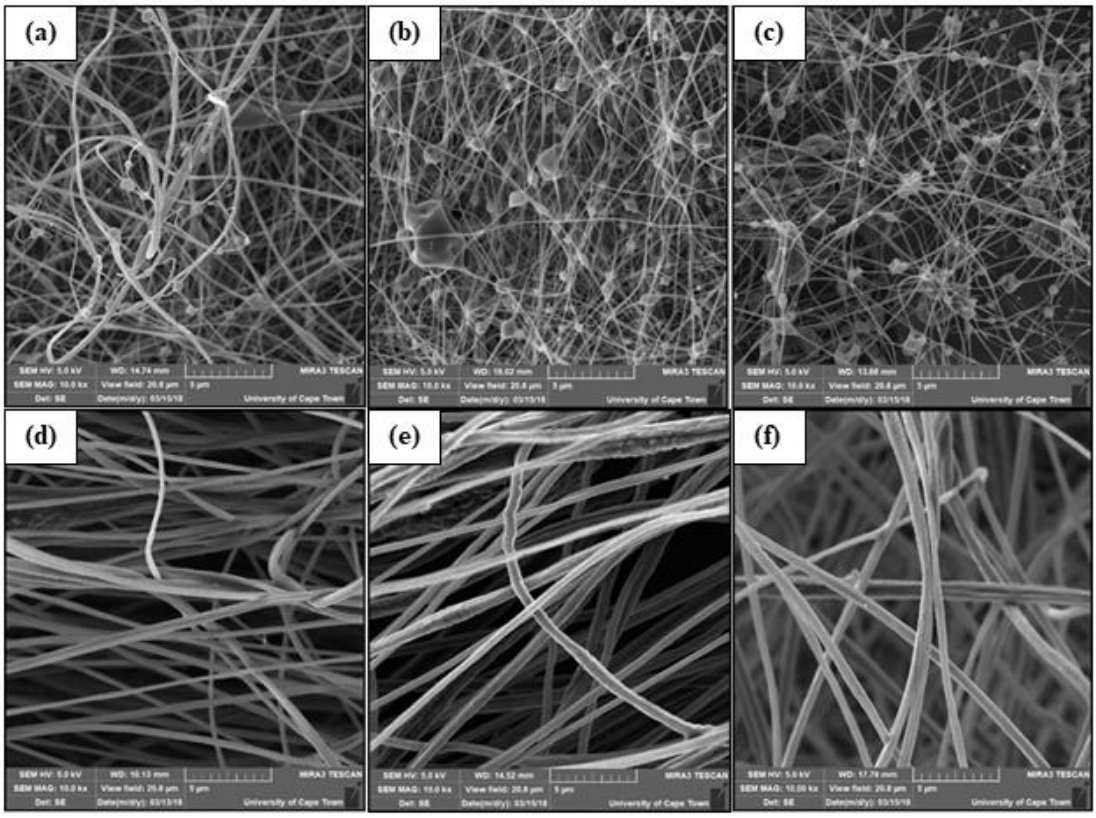

Figure 3.13 SEM images of PAN/CA polymer blends 10/90 (a), 20/80 (b), 30/70 (c), 90/10 (d), 80/20 (e) and 70/30 (f) electrospun at 15 cm distance and 22 kV voltage.

3.2.5. Effect of TiO_2 nanoparticles loading on the blended PAN/CA nanofibers.

To prepare the 80/20 (PAN/CA/TiO_2) composite fibers, different amounts of the nanoparticles were added. The 80/20 PAN/CA blend was the optimum blend to load TiO_2 nanoparticles due to the production of uniform fibers without beads, median size and median amount of CA added to PAN. Figure 3.14 shows the effect of TiO_2 nanoparticles loadings of 1, 2 and 3 wt% on the morphology and diameter of the PAN/CA polymer blended fiber. It was observed that the diameter of the pure 80/20 PAN/CA (538 nm) polymer blended fiber was thicker than that of all the resultant PAN/CA/TiO_2 composite fibers. The 80/20 PAN/CA polymer blend incorporated with TiO_2 nanoparticles (1, 2 and 3 wt%) produced uniform fibers with an increasing average diameter of 207 , 294 and 342 nm, respectively. As the amount of TiO_2 nanoparticles increased from 1 to 3 wt%, the diameter of the fibers linearly increased. Moreover, the addition of the nanoparticles also led to an improved fiber morphology. The improved fiber morphology and reduced fibers diameter

with loading of nanoparticles is due to the increased conductivity and charge density causing the elongation of the polymer jet to form thinner uniform fibers.

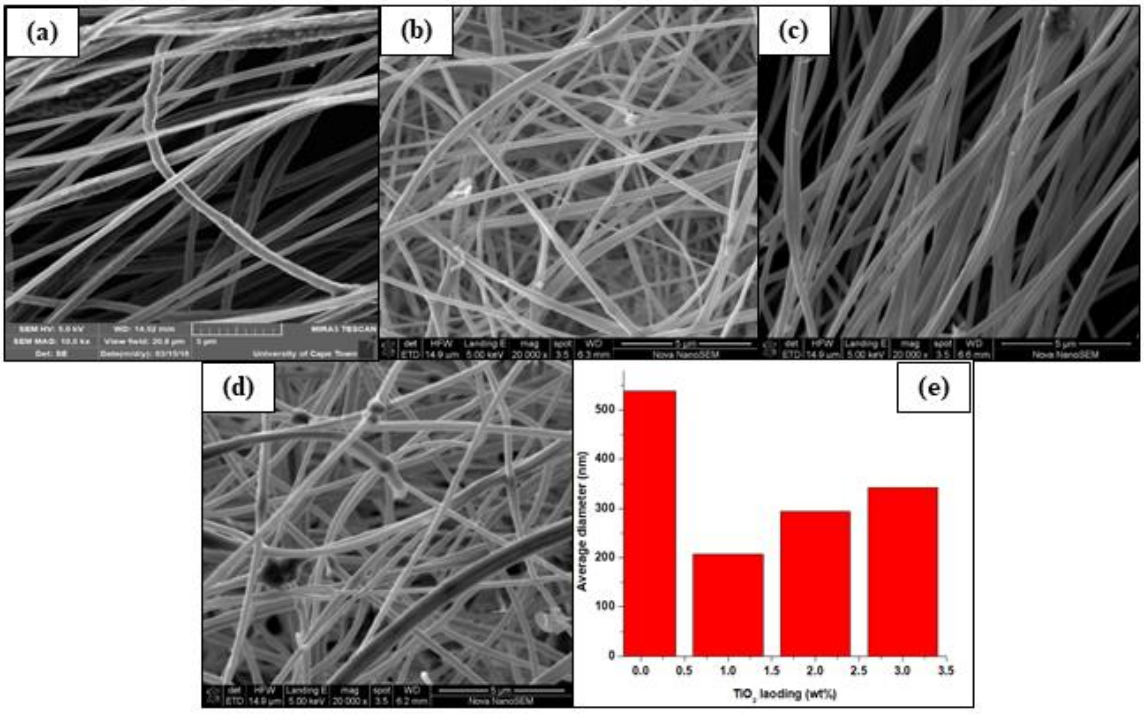

Figure 3.14: SEM images and average fiber diameter distribution (e) of 80/20 PAN/CA polymer blend and different loading of the of TiO_2 nanoparticles 80/20 PAN/CA (a), 1 wt% (b), 2 wt% (c) and 3 wt% (d) Voltage: 22 kV and spinning distance: 15 cm.

3.2.6. EDX analysis of the polymer nanofibers

Figure 3.15 shows EDX spectra obtained from the SEM images of CA-TiO_2, PAN-TiO_2 and PAN/CA-TiO_2 composite fibers. EDX results of CA-TiO_2 nanocomposite did not verify the presence of TiO_2 nanoparticles onto the surface of CA, which may be due to the very low amount of TiO_2 nanoparticles (0.4 wt%) that was incorporated. EDX spectra of PAN-TiO_2 showed that C, O and Ti were the principal elements on the nanocomposite. From the results, it was clear that TiO_2 nanoparticles (2 wt%) were embedded in the PAN-TiO_2 nanocomposites. PAN/CA-TiO_2 EDX results verified that C, O, Ti, Na, Cl elements were homogenously dispersed throughout the composite. The presence of element Cl and Na is due to the use of $TiCl_4$ and NaOH during the

preparation of TiO_2 nanoparticles, respectively. The EDX results provided confirmed the presence of TiO_2 nanoparticles (2 wt%) in the PAN/CA-TiO_2 nanocomposites.

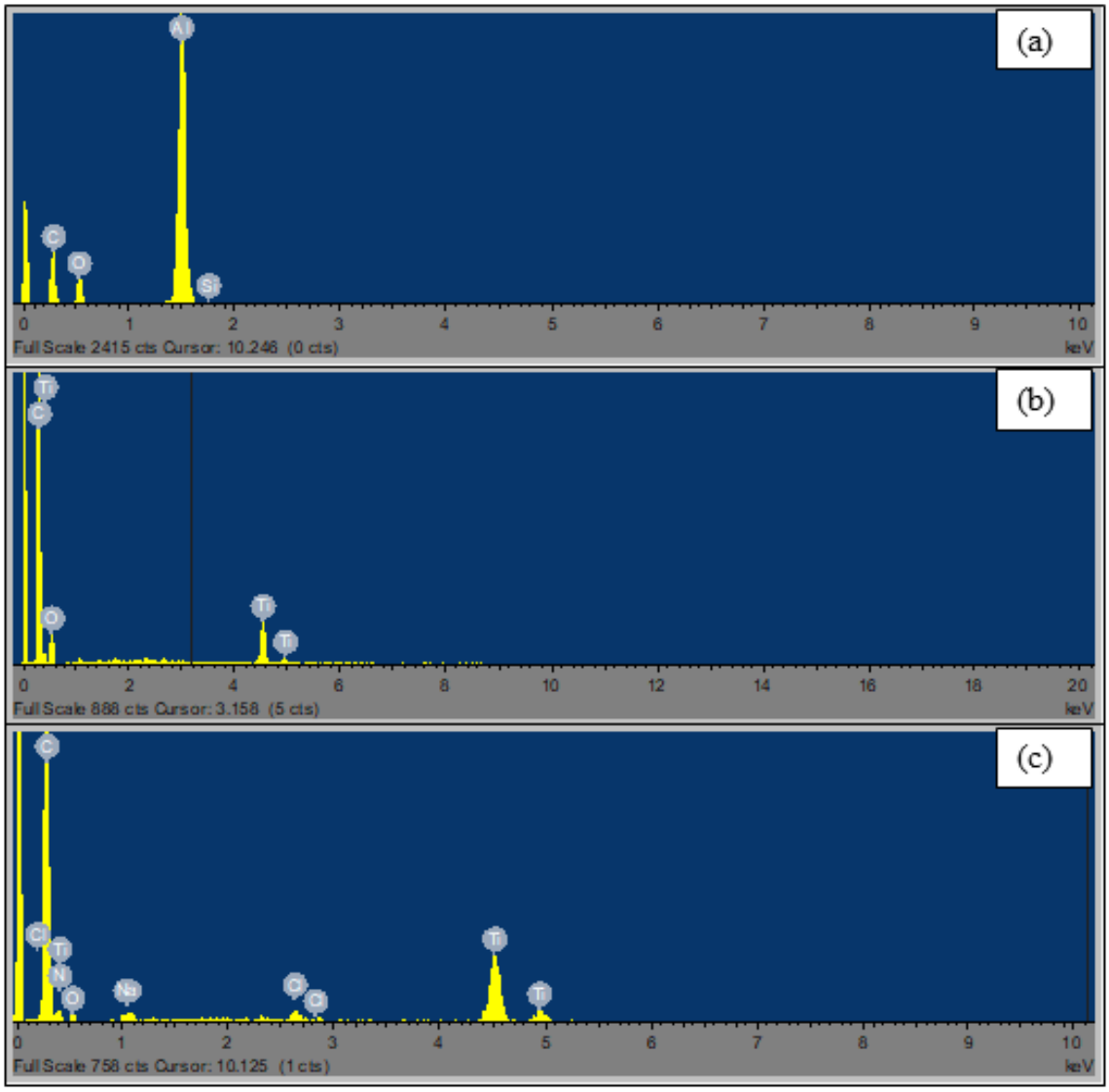

Figure 3.15: EDX spectra of CA-TiO_2 (a), PAN-TiO_2 (b) and PAN/CA-TiO_2 (c).

3.2.7. FTIR spectral analysis of the polymer fibres

Figure 3.16 shows FTIR spectra of pure CA, pure PAN, PAN-TiO_2 and PAN/CA-TiO_2 nanocomposites. The main characteristics bands for PAN were assigned as follows. The peak at 3482 cm^{-1} corresponds to O-H stretching, 2932 cm^{-1} corresponds to C-H stretching in CH and CH_2 group, 2241 cm^{-1} corresponds to the C≡N stretching, 1750 cm^{-1} due to C=O stretching, 1453

cm^{-1} for C-H bending mode and 1054 cm^{-1} corresponds to C-O stretching mode. From the CA spectra, adsorption peak at 3470 cm^{-1} corresponding to the hydroxyl group was observed, 2931 cm^{-1} C-H stretching in CH and CH_2 group was observed, peak at 1739 cm^{-1} can be attributed to the C=O stretching, 1239 cm^{-1} and 1041 cm^{-1} due to CH_3 and ether C-O-C functional groups were observed. Comparing the FTIR spectra of the pure PAN and CA to the PAN/CA blend and PAN/CA-TiO_2 composites, the characteristics peak of O-H group was shifted from 3482 cm^{-1} (PAN) and 3470 cm^{-1} (CA) to 3545 cm^{-1} (PAN/CA) and 3530 cm^{-1} (PAN/CA-TiO_2), respectively. Similar shifts were observed for peaks at 2932 cm^{-1} and 1041 cm^{-1}. The shifts of the peak positions can be attributed to the formation of hydrogen bonding between nanoparticles and matrix. The peak around 500 cm^{-1} corresponds to Ti-O stretching and Ti-O-Ti bands (Riaz et al., 2016).

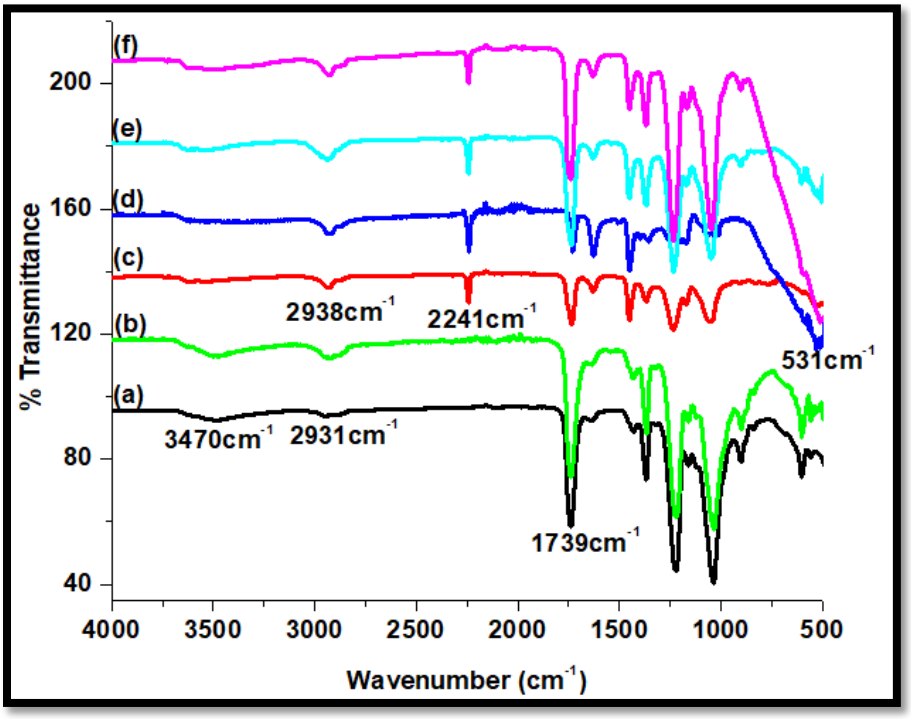

Figure 3.16: FTIR spectra of 16wt% CA (a), CA-TiO_2 (b), 10wt% PAN (c), PAN-TiO_2 (d), PAN/CA (e) and PAN/CA-TiO_2 (f).

3.2.8. XRD analysis of the polymer nanofibers

Figure 3.17 shows the X-ray diffraction patterns of 16wt% CA, 10wt% PAN, CA-TiO_2, PAN-TiO_2, PAN/CA and PAN/CA-TiO_2. The CA nanofibers reveals two broad amorphous peaks in the

range of 2Θ=15.0-25.8º and 29.7-40.1º which corresponds to its crystalline nature. The CA nanofibers immobilized with TiO_2 nanoparticles are similar to that of pure CA nanofibers except the diffraction peak that appears at 33.9º corresponding with 002 plane. The broad peaks centered at 2Θ=20º and 34º observed for PAN and PAN-TiO_2 reveals the amorphous nature of PAN. PAN-TiO_2 exhibited a diffraction peak of 2Θ=33.9º corresponding with 002 plane. The amount of actual TiO_2 nanoparticles immobilized onto the polymer were most likely too low to be detected using XRD technique.

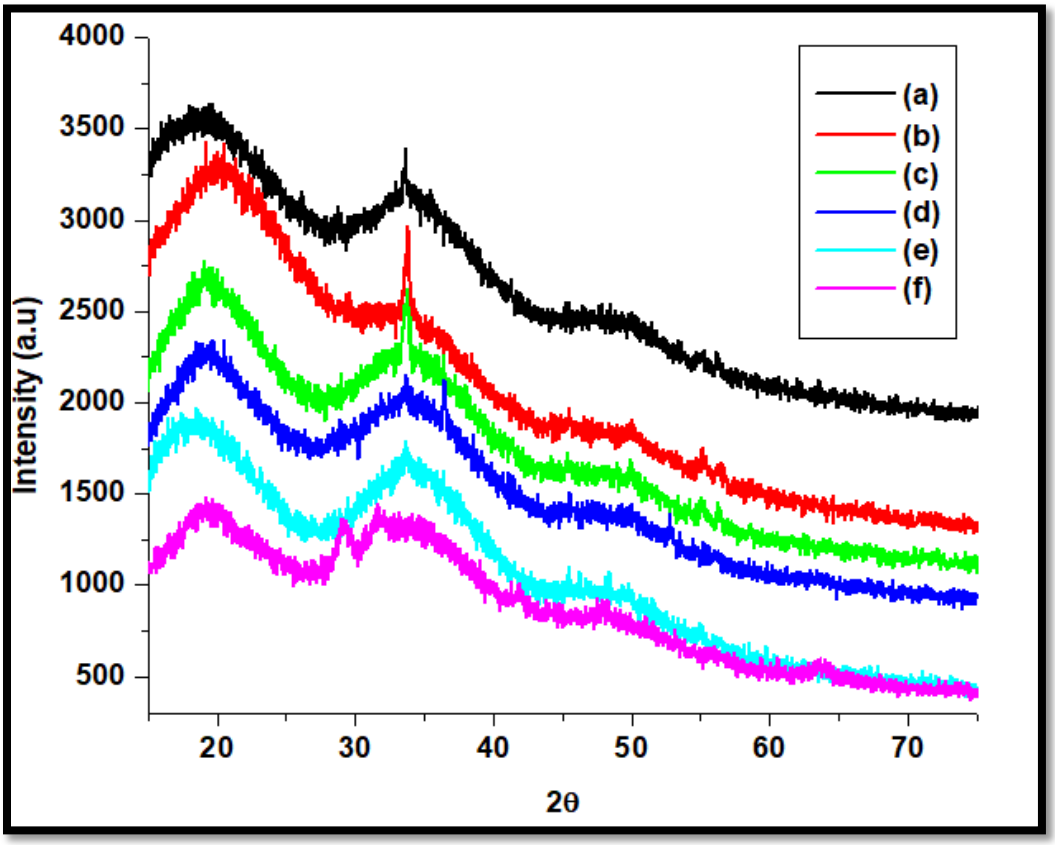

Figure 3.17: XRD patterns of 16 wt% CA (a), CA-TiO_2 (b), PAN-TiO_2 (c), 10 wt% PAN (d), PAN/CA (e) and PAN/CA-TiO_2 (f).

The electrospun PAN/CA blended nanofibers reveal the two broad peaks that were observed for both the pure PAN and pure CA nanofibers which correspond to their crystalline nature. The

PAN/CA-TiO_2 exhibited diffraction peaks around at 28.9º, 31.8º, 41.8º, 48.0º and 64º, corresponding to the (110), (121), (111), (200) and (310) crystal planes of TiO_2, respectively.

3.2.9. TGA analysis of the polymer nanofibers

Figure 3.18 displays the thermogravimetric analysis of the electrospun composite nanofibers in the temperature range of 30–800 °C using 10 mg samples with a heating rate of 10 °C/min under a nitrogen purge at a rate of 10 mL/min. The yield residual mass for CA at 800 °C was 12.7% and the initial mass reduction was 3.6% weight loss up to 274 °C attributed to the evaporation of water and solvent molecules. The second weight loss was from 274 °C to 418 °C, it was attributed to cellulose pyrolysis. 17.8% unburned carbonaceous resedue was found at 418 °C.

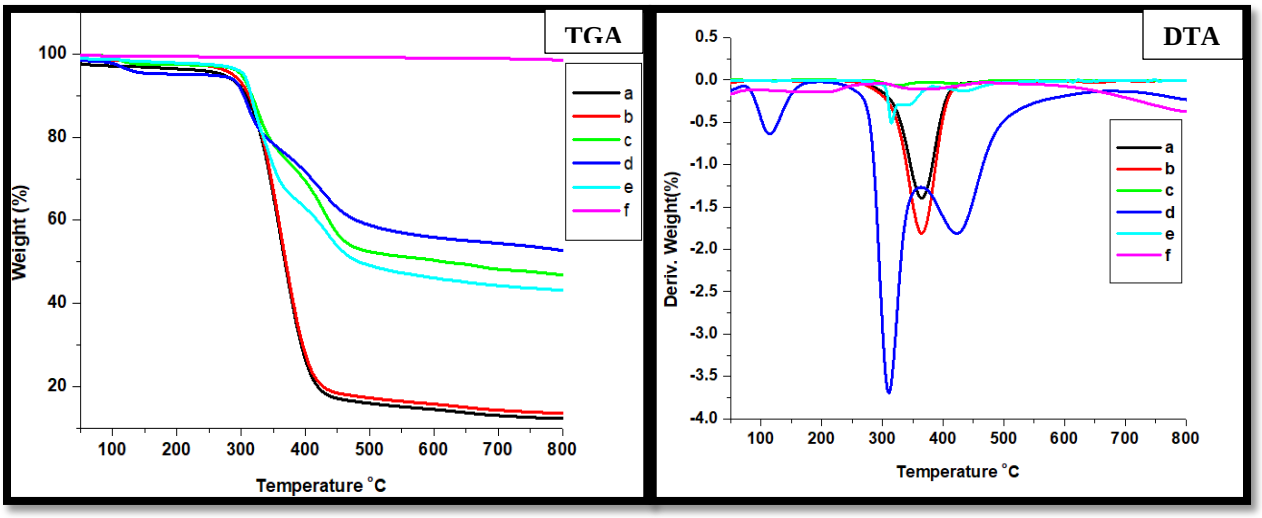

Figure 3.18: TGA and DTA curves of 16 wt% CA (a), CA-TiO_2 (b), PAN-TiO_2 (c), 10 wt% PAN (d), PAN/CA (e) and PAN/CA-TiO_2 (f).

The TGA curve for CA-TiO_2 has yielded residual mass of 13.2% at 800 °C and the first mass reduction began at 286°C associated with the evaporation of water. The second degradation occurred from 286 °C up to 420 °C associated with the main thermal degradation reaction of CA. The TGA curve of CA and CA-TiO_2 were almost the same due to the less amount of TiO_2 nanoparticles incorporated. The PAN nanofibers first weight loss was 2.5% from 121 °C to 338 °C. From 338 to 358 °C, the TGA curve showed 21% weight of residue associated with cyclization

of nitrile groups in PAN polymer chain (Karki et al., 2019). From 358 to 474 °C, the TGA curve showed 44% weight loss which might be related to thermal degradation reaction of PAN and the yield residual mass for PAN at 800 °C was 52.5%. The PAN-TiO_2 nanofibers first weight loss was 4.8% from 115 to 144 °C. From 144 to 293°C, the weight of PAN was almost unchanged. 19% weight loss up to 352 °C associated with opening of triple bonds. From 352 to 460 °C, the TGA curve showed 46% weight of residue associated with decomposition reaction of PAN. The crystallinity of the PAN nanofibers is reduced due to the presence of the nanoparticles. There was almost no change in weight of PAN/CA blended nanofiber up to the temperature 321 °C and the initial mass reduction was 32% weight loss up to 362 °C which was attributed to the cyclization of the nitrile group since the blend is dominated by PAN. From 362 to 468 °C, the TGA curve showed 47% weight loss which showed improved thermal stability of the blend. The yield residual mass for PAN/CA at 800 °C was 56% which shows that the blended nanofibers has thermal properties of both CA and PAN as desired during fabrication of the PAN/CA blended nanofibers. No weight loss was observed for PAN/CA-TiO_2 nanofibers, showing that a stable metal oxide with well developed Ti-O-Ti chain was attained improving the stability of the composite nanofibers (Mutuma et al., 2015). Diffractional thermal analysis (DTA) provides detailed information on the polymer decomposition temperature.

3.3. Antibacterial activity of the polymer nanofibers

The antibacterial activity of electrospun pure PAN, pure CA, PAN/CA blended nanofibers, PAN-TiO_2 and PAN/CA-TiO_2 nanofibers were carried out by zone of inhibition assay using the agar plate method against bacterial strain. *E Coli, S. aureus* and *C. albicans* fungi and is shown in Figures 3.19, 3.20 and 3.21. Figure 3.19 reveals that pure PAN, pure, CA and PAN/CA blended nanofibers had no zone of inhibition against *E. col*i and *C. albicans* which can be due to their non-bactericidal property against these bacterial strains. Moreover, pure PAN, pure CA and PAN/CA blended nanofibers showed some minor inhibition zone against *S. aureus*.

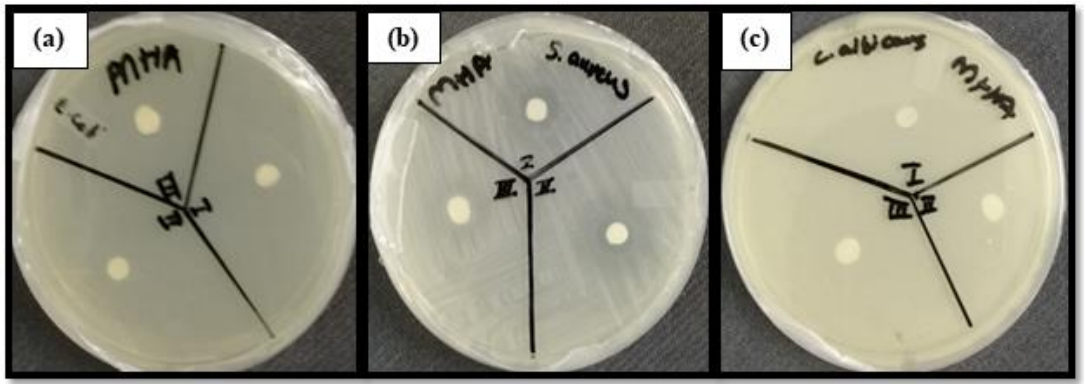

Figure 3.19: The inhibition zone of pure PAN (I), pure CA (II) and PAN/CA blended nanofiber (III) against *E. coli* (a), *S. aureus* (b) and *C. albicans* (c).

In Figure 3.20, the zone of inhibitions were clearly observed for PAN-TiO_2 only against *E. coli* and *C. albicans* not *S. aureus*, this shows that *S. aureus* was the least sensitive microbe against antimicrobial PAN-TiO_2 nanofibers. Inhibition zones were clearly observed from Figure 3.21 for all the PAN/CA-TiO_2 composites and the inhibition zone of the PAN/CA-TiO_2 composites against *E. coli* were larger than the other bacterial strains. The result indicate that the combination of TiO_2 nanoparticles with PAN and PAN/CA blended nanofibers enhance the antibacterial properties against *E Coli, S. aureus* and *C. albicans*. PAN/CA-TiO_2 showed improverd activity against both the bacterial strains and the fungi.

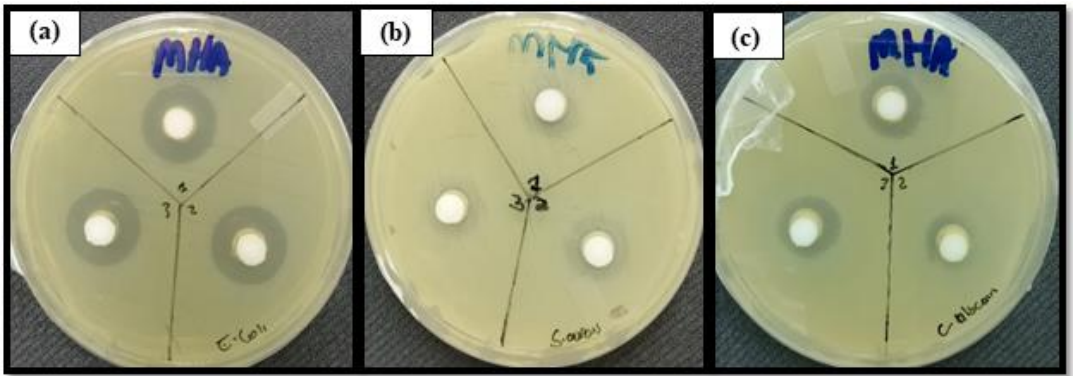

Figure 3.20: The inhibition zone of PAN-TiO_2 (1%, 2% and 3% TiO_2) against *E. coli* (a), *S. aureus* (b) and *C. albicans* (c).

The different loadings of TiO_2 nanoparticles on the fibers did not have any obvious trend on antimicrobial activity. As seen in all the results, PAN/CA-TiO_2 nanofibers have great potential to be used as antimicrobial agents for water purification. Table 2 shows the diameter inhibition zone (mm) of electrospun nanofibers against *E. coli*, *S. aureus* and *C. albican*. The results revealed that PAN/CA-TiO_2 nanocomposite fibers have sufficiently higher antibacterial properties than the other nanomaterials. *E. coli* was the most sensitive microbe and *S. aureus* was the least sensitive microbe against all tested antimicrobial agents. Overall, the prepared PAN-TiO_2 and PAN/CA-TiO_2 nanocomposite have been demonstrated to be effective and useful in the bactericidal application and may be a reasonable alternative for development of new antimicrobial agents. However, the use of the fibers in solid form should be strengthened in future in order to overcome the challenge associated with the use of the solid fibers which requires a different approach to adapt.

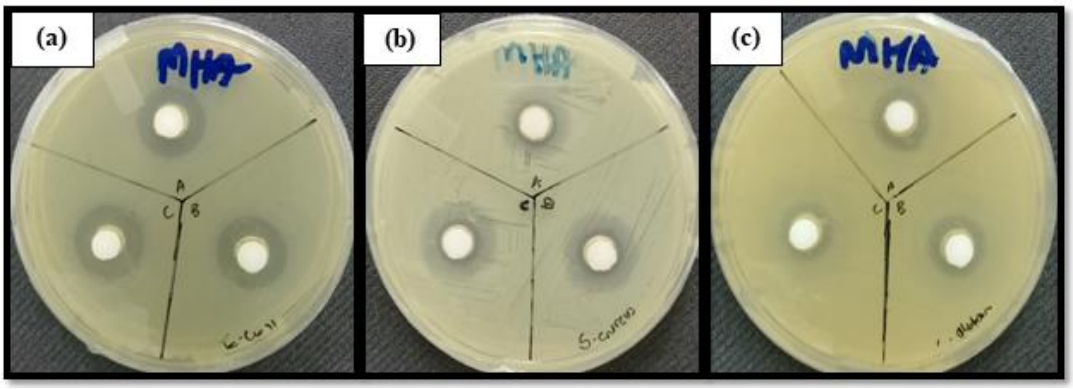

Figure 3.21: The inhibition zone of PAN/CA-TiO_2 (1%, 2% and 3% TiO_2) against *E. coli* (a), *S. aureus* (b) and *C. albicans* (c).

Table 2. Inhibition zone (mm) of electrospun nanofibers against *E. coli*, *S. aureus* and *C. albican.*

Nanomaterials	Zone of Inhibition (mm)		
	E.coli	*S. aureus*	*C. albicans*
PAN	0	3.1	0
CA	0	1.4	0
PAN/CA	0	0	0
PAN-TiO_2 1%	19.3	0	16.8
PAN-TiO_2 2%	20.1	0	7.6
PAN-TiO_2 3%	19.2	0	14.9
PAN/CA-TiO_2 1%	22.3	17.8	19.2
PAN/CA-TiO_2 2%	22.2	21.7	18.4
PAN/CA-TiO_2 3%	24.4	20.2	10.1

3.4. Photocatalytic degradation using polymer nanofibers

The photocatalytic activities of the synthesised TiO_2 nanoparticles, PAN/-TiO_2 and PAN/CA-TiO_2 nanofibers were determined using Methyl orange aqueous solutions as a model organic dye under natural light. Methyl orange is a common azo dye with features of both a dye and acid-based indicator in aqueous solution (Yang et al., 2017) . The characteristic maximum absorption peak of methyl orange was at 466 nm and the UV-vis absorption spectra of TiO_2 nanoparticles was at 325 nm. The degradation of the dye is represented by the UV-vis spectra of methyl orange solution as a function of time. Figures 3.22, 3.23 and 3.24 show the UV-vis spectra of Methyl orange in the presence of TiO_2 nanoparticles, PAN-TiO_2 and PAN/CA-TiO_2 nanofibers, respectively. Furthermore, their removal efficiency graphs are presented in Figures 3.25. The UV-vis spectra for the degradation of methyl orange in the presence of TiO_2 nanoparticles in Figure 3.22 showed minimum change in the absorption peak with the evolution of the reaction time. The spectra for MO showed that the intensity of the peak at maximum absorption of the dye diminished as the contact time increased from 0 to 300 minutes. This can be due to the negligible contact of the total surface area of TiO_2 nanoparticles and methyl orange, whereby some of the nanoparticles were encapsulated meaning that their contact with the pollutant was not direct. Moreover, the saturation

point was reached due to the surface active sites of TiO_2 nanoparticles being fully occupied by methyl orange (Panayotov & Morris, 2016). Hense, less active sites of TiO_2 nanoparticles were available for further adsorption.

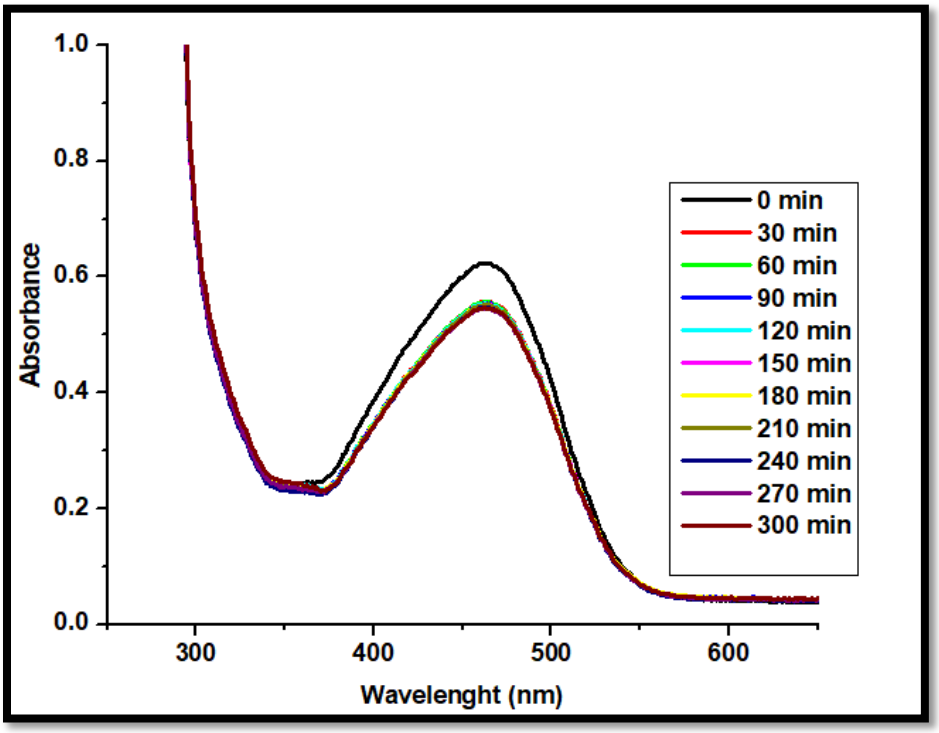

Figure 3.22: UV-vis absorption spectra of methyl orange in the presence of TiO_2 nanoparticles using time variation.

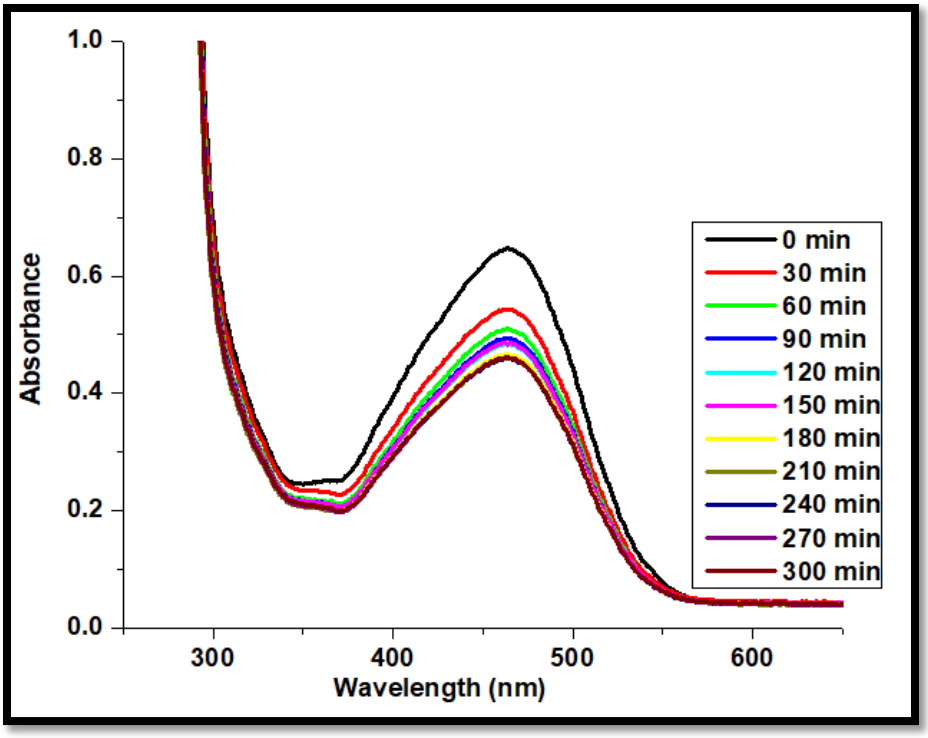

Figure 3.23: UV-vis absorption spectra of methyl orange in the presence of PAN-TiO_2 nanofibers using time variation.

Figure 3.23 shows the UV-vis absorption spectra of methyl orange in the presence of PAN-TiO_2 nanofibers. From the results, improvement of degrading MO was observed by incorporating TiO_2 nanoparticles onto PAN polymer, thus, this confirmed PAN as a potential adsorbent. The interaction between the adsorbate and the surface sites of the adsorbent was improved because both PAN and methyl orange are polar, hence, PAN is a promising support for photocatalysts as an adsorbent (Nyamukamba et al., 2016).The increased number of catalytic sites on the surface of TiO_2 nanoparticles activates the adsorption of substance enhancing the photocatalytic activity. The higher photocatalytic activity of TiO_2 nanoparticles is due to the calcination of the nanoparticles which increases the crystallinity and phase transformation resulting in a mixture of the anatase and rutile phase. Crystallinity and mixture of phase improves the photocatalytic activity of TiO_2 nanoparticles. The rate of degradation decreased significantly with the increased contact time from 60 to 300 minutes. This decrease is attributed to the less surface active site of TiO_2 nanoparticles available for further adsorption and redused light absorption capacity.

Figure 3.24 revealed that the photocatalytic degradation rate of MO in the presence of PAN/CA-TiO_2 were higher than that of PAN/-TiO_2. This indicates that blending of PAN and CA improves the mechanical strength of the polymer in water, hence, the blend matrix was used as a support for the photocatalyst and an adsorbant. The absorbant content is increased by blending PAN with CA due to the hydroxyl functional group of CA and the amine group of PAN (Gupta et al., 2013; Chauque et al., 2017). This signified that polymer nanofibers are better support for photocatalyst as adsorbant because they bring contaminants closer to the photocatalyst to be degraded. Furthermore, the photocatalytic activity of the nanofiber composite is improved by the presence of TiO_2 nanoparticles due to the higher surface area and porosity, hydroxyl group and band gap. Electron hole pair generation is improved by the increased band gap. The presence of the hydroxyl group play an important role of attacking the contaminates in water. The higher surface accommodates the hydroxyl group enhancing the degradation rate (Tayade et al., 2007). The absorption spectra of methyl orange in the presence of PAN/CA-TiO_2 nanofibers showed rapid degradation from 0 to 30 and then to 60 minutes. This was attributed to the adsorption of MO on TiO_2 nanoparticles and the presense of the porous structures in the PAN/CA-TiO_2 nanofibers photocatalysts. The pores of PAN/CA-TiO_2 nanofibers functioned as conduit for the transport of MO from the outer surface to the inner surface of the PAN/CA-TiO_2 nanofibers photocatalysts. As time increased from 90 to 300 minutes the degradation of MO became very slow due to the exclusion of MO to adsorb on the interior surface of PAN/CA-TiO_2 nanofibers and the surface active sites of TiO_2 nanoparticles being fully occupied by MO.

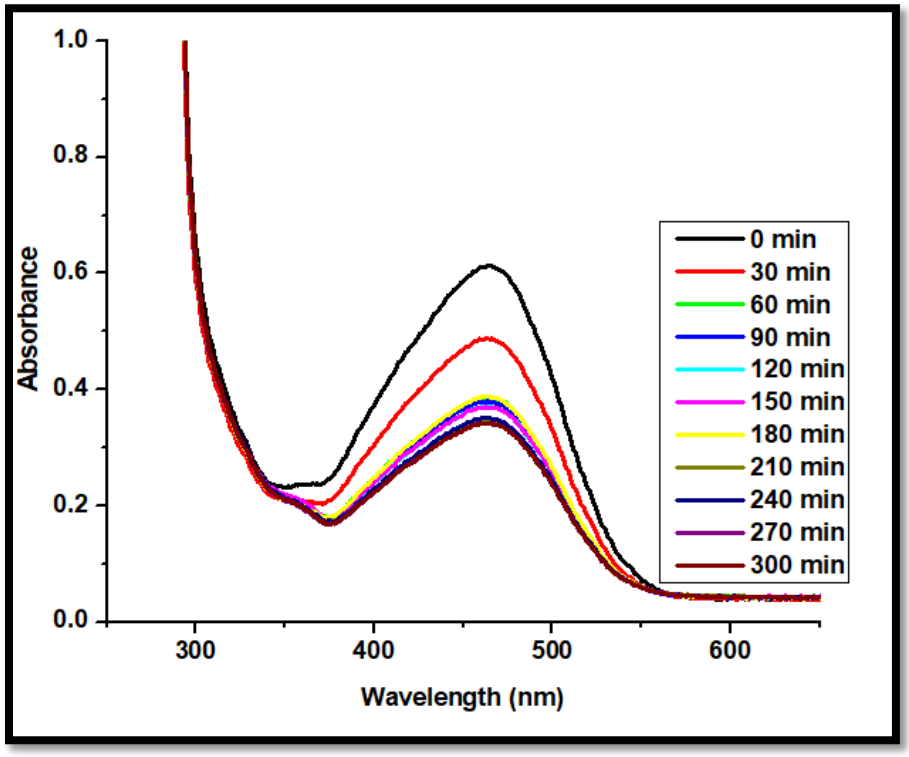

Figure 3.24: UV-vis absorption spectra of Methyl orange in the presence of PAN/CA-TiO_2 nanofibers using time variation.

Figure 3.25 shows the removal efficiency of methyl orange by TiO_2 nanoparticles, PAN-TiO_2 and PAN/CA-TiO_2. The removal efficiency of MO by TiO_2 nanoparticles was found to be 10.7% within 30 min contact time, which stayed more or less the same even after 300 min of contact time. This signifies the poor removal of MO by TiO_2 nanoparticles. PAN-TiO_2 showed improved photocatalytic degradation of MO as compared to TiO_2 nanoparticles with 21.2% removal efficiency within 60 min, followed by a removal efficiency of 32% within 270 min. PAN/CA-TiO_2 was the most effective nanomaterial compared to the others with removal efficiency of 37% within 60 min , followed by 43% removal efficiency within 210 min. This observations show that PAN/CA-TiO_2 nanofibers have good adsorption capacity, therefore, enhancing the photocatalytic activity of TiO_2 nanoparticles. The improved mechanical strength of the nanofiber composite allows the material to be reused and easily removed from water. From these results, it can be deduced that the performance of PAN-TiO_2 and PAN/CA-TiO_2 nanofibers can further be improved to degrade MO with increased time since the graph is not flattening out as compared to that of TiO_2 nanoparticles.

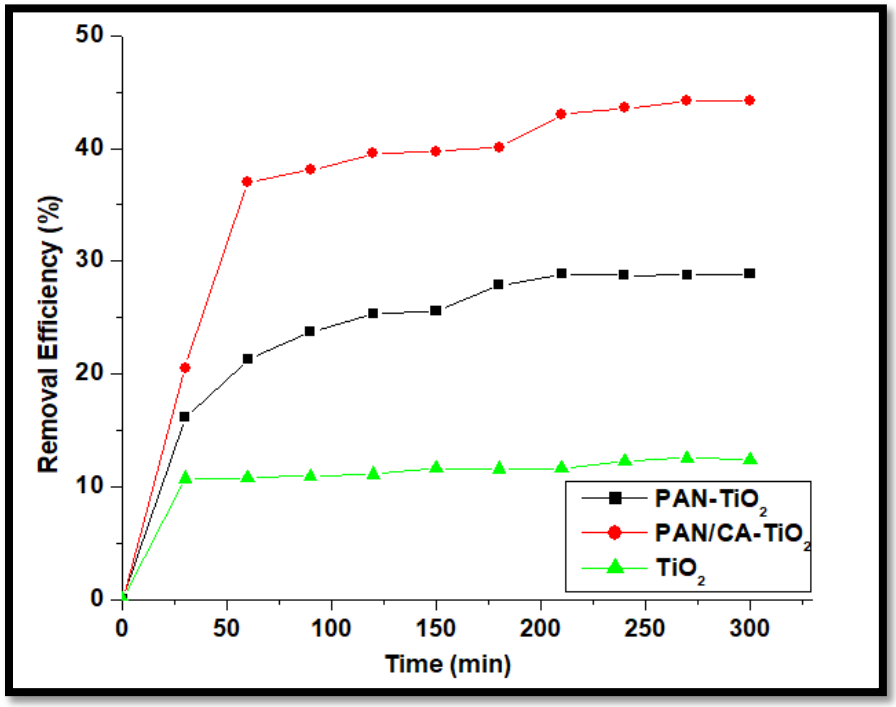

Figure 3.25: Removal profile of methyl orange by TiO_2 nanoparticles, PAN-TiO_2 and PAN/CA-TiO_2.

Chapter 4
Conclusions and Recommendations

4.0. Conclusions and Recommendations

This chapter gives the genral conclusions of the whole study of TiO_2 nanoparticles, PAN/CA blended nanofibers and PAN/CA-TiO_2 composite nanofibers as well as their antibacterial and photodegradation tests. Finally, recommendations based on further work that can be done on this study are outlined.

4.1. Conclusions

Sol-gel method was used to prepare TiO_2 nanoparticles and the calcination temperatures were varied to produce TiO_2 nanoparticles with increased crystallite size, average particle size and anatase phase content. The sol-gel method makes it possible to synthesise nanoparticles with desired structural characteristics such as morphology, diameter and porosity by controlling the parameters such as temperature and pH. The successfully synthesised TiO_2 nanoparticles were analysed using UV-Vis, PL, FTIR spectroscopy, TEM and XRD. UV-vis spectroscopy confirmed that the TiO_2 nanoparticles formed are nanosized with extended optical band edge. TEM results showed spherical TiO_2 nanoparticles with increased particle size. XRD illustrates the increased crystallite size due to the increase in particle size with increasing calcination temperature. The FTIR spectra confirmed that indeed TiO_2 nanoparticles have been formed as demonstrated by the peak at around 500 cm^{-1} corresponding to Ti-O stretching and Ti-O-Ti bands . The electrospinning technique was used for the fabrication of PAN/CA blended nanofibers and the immobilization of the TiO_2 nanoparticles onto the polymer blended nanofibers. SEM images showed the morphology and size of the fabricated nanofibers. The blending of the PAN and CA polymers was confired by the SEM images and the FTIR spectra. The nanofiber had uniform distribution without beads at optimum concentration, distance and applied voltage. The FTIR spectra and SEM-EDS confirmed the presence of TiO_2 nanoparticles onto the polymer blended nanofibers.

The synthesised nanofiber composite were tested for antimicrobial activity against *E. coli*, *S. aureus* and *C. albicans* microorganisms. The antimicrobial activity results in showed that the pure

PAN, CA and PAN/CA nanofibers had no effect against *E. col*i and *C. albicans* but showed minor inhibition zone against *S. aureus*. PAN-TiO_2 and PAN/CA-TiO_2 had improved antimicrobial activity against the selected microorganisms showing great potential to be used as antimicrobial agent. Furthuremore, the synthesised TiO_2 nanoparticles and nanofiber composites were tested for photocatalytic activity using methyl orange as a model pollutant. The photocatalytic activity results showed good performance by the nanofiber composite for the removal of methyl orange because of the enhanced degradation of the dye. The antimicrobial actictivity and photocatalytic actictivity results showed that the increased calcination temperature of the synthesised TiO_2 nanoparticles improved the crystallinity which enhanced the antimicrobial actictivity and photocatalytic actictivity of the nanofiber composites. The photocatalytic observations were due to the immobilization of nanoparticles onto the polymer nanofibers that enabled the traping of photogenerated electrons, therefore, preventing recombination of electron hole pairs. The improved machanical properties of two blended polymer allows the nanofiber composites to be easily removed from the dye solution. Moreover, the polymer nanofibers were used as a support because of their high adsorption capacity.

4.2. Further work and recommendations

Further work is recommended for this research to answer the questions that arose from this study as well as additional investigation on optimization of some of the parameters. Doping titania with silver and immobilizing the nanoparticles onto the polymer blended fibres to compare their antimicrobial and photocatalytic activities against the undoped titania-nanofiber composite. The distribution or spread of TiO_2 nanoparticles on polymer blended nanofibers could also be determined using TEM with capacity to analyse the metals or metal oxide. Increasing the applied voltage gap to 4kV on the electrospinning of the polymer nanofibers to determine if this change will have effect on the morphology and diameter. Instead of using natural light for photodegradation of model organic pollutants, UV light should be utilized. The photocatalytic activity of the nanofiber composites should be investigated on other model organic pollutants such as methylene blue (MB) and congo red (CR).

References

AHMAD, R. & SARDAR, M. (2013). TiO_2 nanoparticles as an antibacterial agents against *E. coli*. *International Journal of Innovative Research in Science, Engineering and Technology*. 2(8). p. 3569-3574.

AMOABENG, D., ROELL, D., CLOUSE, M., YOUNG B.A. & VELENKAR, S.S. (2017). A composition- morphology map for particles- filled blends of immiscible thermoplastic polymers. *Journal of Polymer*. 119. p. 212-213.

ANU, M.E. & SARAVANAKUMAR M.P. (2017). A review on the classification, characterization, synthesis of nanoparticles and their application. *Journal of Materials Science and Engineering*. 263 (2017). p. 1-15.

AZIN, K., MALIHE, H., NARGES, A. &AHMAD KERMANPUR. (2016). Characterization of pure Ni ultrafine nanoparticles synthesised by electromagnetic levitation gas condensation method. *Journal of Material Research Bulletin*. 74. p. 212-217.

BAJI, A., MAI, Y., WONG, S., ABTAHI, I. & CHEN, P. (2010). Electrospinning of polymer nanofibers: effect on oriented morphology, structures and tensile properties. (2010). *Journal of Composites Science and Technology*. 70 (2010). p. 703–718.

BAKAR, S.S.S., FONG, K.C., ELEYAS, A. & NAZERI, M.F.M. (2018). Effect of voltage and flow rate electrospinning parameters on polyacrylonitrile electrospun fibers. *Journal of Materials Science and Engineering*. 318 (2018). p. 1-7.

BEACHLEY, V. & WEN, X. (2008). Effect of electrospinning parameters on the nanofiber diameter and length. *Journal Materials Science and Engineering C*. 29 (2009). p. 663–668

BOGNITZKI, M., CZADO, W., FRESE, T., SCHAPER, A., HELLWIG, A., STEINHART, M., GREINER, A. & WENDORFF, J.H. (2001). Nanostructured fibers via electrospinning. *Journal of Advance Materials*. 13 (2001). p. 70-72.

CHAUQUE, E.F.C., DLAMINI, L.N., ADELODUN, A.A., GREYLING, C.J. & NGILA, J.C. (2017). Electrospun polyacrylonitrile nanofibers functionalized with EDTA for adsorption of ionic dyes. *Journal of Physics and Chemistry of the Earth*. 100 (2017). p. 201-211.

CHEN, Q., LIU, H., XIN, Y. & CHENG, X. (2013). TiO_2 nanobelts- Effect of calcination temperature on optical, photoelectrochemical and photocatalytic properties. *Journal of Electrochimica Acta*. 111 (2013). p.284-291.

CHEN, W., SU, Y., ZHENG, L., WANG, L. & JIANG, Z. (2009). The improved oil/water separation performance of cellulose acetate-graft-polyacrylonitrile membranes. *Journal of Membrane Science*. 337 (2009). p. 98-105.

CHOWDHURY, M. & STYLIOS, G. (2010). Effect of experimental parameters on the morphology of electrospun nylon 6 fibres. *International Journal of Basic & Applied Sciences*. 10 (06). p. 70-78.

DANIAL, A. CERQUEIRA, ARKUR, J.M. VALENTE, GUIMES, R. FILHO & HUGH, D. BURROWS. (2009). Synthesis and characterization of blends of polyaniline and cellulose acetate obtained from sugarcane bagasse waste. *Journal of Carbohydrate Polymers*. 78 (3). p. 402-408.

DONG, F., ZHAO, W., WU, Z. & GUO, S. Band structure and visible light photocatalytic activity of multi-type nitrogen doped TiO_2 nanoparticles prepared by thermal deposition. *Journal of Hazardous Materials*. 162 (2009). p. 763-770.

DUBEY, R.S. (2017). Temperature-dependent phase transformation of TiO_2 nanoparticles synthesised by sol-gel method. *Journal of Materials Letters*. 215 (2018). p. 312-317.

GOETZ, L.A., JALVO, B., ROSAL, R. &MATHEW, A.P. (2016). Superhydrophilic anti-fouling electrospun cellulose acetate membranes coated with chitin nanocrystals for water filtration. *Journal of Membrane Science*. 510 (2016). p. 238-248.

GUPTA, S. & TRIPATHI M. (2011). A review of TiO_2 nanoparticles. *Journal of Chinese Science Bulletin*. 56 (16). p. 1639-1657.

GUPTA, V.K., PATHANIA, D., SINGH, P., RATHORE, B.S. & CHAUHAN, P. (2013). Cellulose acetate–zirconium (IV) phosphate nano-composite with enhanced photo-catalytic activity. *Journal of Carbohydrate Polymers*. 95 (2013). p. 434-440.

HAGGERTY, J.E.S., SCHELHAS, L.T., KITCHAEV, D.A., MANGUM, J.S., GARTEN, L.M., SUN, W., STONE, K.H., PERKINS, J.D., TONEY, M.F., CRDER, G., GINLEY, D.S., GORMAN, B.P. & TATE, J. (2017). High- friction brookite films from amorphous precursors. Journal of Science Reports. 15232 (2017). p. 1-11.

HAIDER, A., HAIDER, S. & KANG, I. (2018). A comprehensive review summarizing the effect of electrospinning parameters and potential applications of nanofibers in biomedical and biotechnology. *Arabian Journal of Chemistry*. 11 (8). p. 1165-1188.

HAIDER, S., AL-ZEGHAYER, Y., AHMED ALI, F.A., HAIDER, A., MAHMOOD, A., AL-MASRY, W.A., IMRAN, M. & AIJAZ, M.O. (2013). Highly aligned narrow diameter chitosan electrospun nanofibers. *Journal of Polymer Research*. 20 (105). p. 1-11.

HAO, J., LIA, W., SUOA, X., WEIA, H., LUC, C. & LIUA, Y. (2018). Highly isotactic (>60%) polyacrylonitrile-based carbon fiber: Precursor synthesis, fiber spinning, stabilization and carbonization. *Journal of polymer*. 157 (2018). p. 139-150.

HAORAN, D., GUANGMING, Z., LIN, T., CHANGZHENG, F., CHANG, Z., XIAOXIAO, H. & YAN H. (2015). An overview on limitations of TiO_2- based particles for photocatalytic degradation of organic pollutants and the responding countermeasures. *Journal of Water Research*. 79. p.128-146.

HAYLE, S.T. & GONFA, G.G. (2014). Synthesis and characterization of titanium oxide nanomaterials using sol-gel method. *American Journal of Nanoscience and Nanotechnology*. 2 (1).p. 1-7.

HE, C., LIU, J., LI, J., ZHU, F. & ZHAO, H. (2018). Blending based polyacrylonitrile/poly(vinyl alcohol) membrane for rechargeable lithium ion batteries. *Journal of Membrane Science*. 560 (2018). p. 30-37.

HEIKKILA, P. & HARLIN, A. (2008). Parameter study of electrospinning of polyamide-6. *European Polymer Journal*. 44 (2008). p. 3067–3079.

HIR, Z. A. M., MORADIHAMEDANI, P., ABDULLAH, A.H. & MOHAMED, M.A. (2017). Immobilization of TiO_2 into polyethersulfone matrix as hybrid film photocatalyst for effective degradation of methyl orange dye. *Journal of Materials Science in Semiconductor Processing*. 57 (2017). p. 157-165.

HUEI-SIOU, C., CHAOCHIN, S., JI-LIAN, C., TSAI-YIN, Y., NAI-MU, H. & WEN-REN, L. (2011). Preparation and characterization of pure rutile TiO_2 nanoparticles for photocatalytic study and thin films for dye-sensitized solar cell. *Journal of Nanomaterials*. 2011. p. 8.

HUEI-SIOU, C., CHAOCHIN, S., JI-LIAN, C., TSAI-YIN, Y., NAI-MU, H. & WEN-REN, L. (2010). Preparation and characterization of pure rutile TiO_2 nanoparticles for photocatalytic study and thin films for dye-sensitized solar cell. *Journal of Nanomaterials*. 2011. p. 8.

KHAN, I., SAEED, K. & KHAN, I. (2017). Nanoparticles: Properties, applications and toxicities. *Arabian Journal of Chemistry*. p. 1-24.

IRAVANI, S., KORBEKANDI, H., MIRMOHAMMADI, S.V. & ZOLFAGHARI, B. (2014). Synthesis of silver nanoparticles: chemical, physical and biological method. *Journal of Research in Pharmaceutical Sciences*. 16 (9). p. 385-406.

JYOTISHKUMAR, P., SABU, T. & YVES, G. (2015). *Characterization of polymer blends: miscibility, morphology, and interfaces*. Priyadarshini Hills P.O. 686-560 Kottayam, Kerala India: Wiley-VCH Verlag GmbH & Co. KGaA.

KARKI, H.P., KAFLE, L., OJHA, D.P., SONG, J.H. & KIM, H.J. (2019). Cellulose/polyacrylonitrile electrospun composite fiber for effective separation of the surfactant-free oil-in-water mixture under a versatile condition. *Journal of Separation and Purification Technology*. 210 (2019). p. 913-919.

KEITEB, A.S., SAION, E., ZAKARIA, A., SOLTANI, N. & AND ABDULLAHI, N. (2016). A modified thermal treatment method for the up-scalable synthesis of size-controlled nanocrystalline titania. *Journal of Applied Sciences*. 6 (295). p. 1-10.

KHARAGHANIA, D., JOB, Y.K., KHANA, M.Q., JEONGB, Y., CHAB, H.J. & KIMA, I.S. (2018). Electrospun antibacterial polyacrylonitrile nanofiber membranes functionalized with silver nanoparticles by a facile wetting method. *European Polymer Journal*. 108 (2018). p. 69-75.

KUMAR, P.S., VENKATESH, K., GUIA, E., SUNDARAMURTHYA, J., SINGHA, G. & ARTHANAREESWARAN, G. (2018). Electrospun carbon nanofibers/TiO_2-PAN hybrid membranes for effective removal of metal ions and cationic dye, *Journal of Environmental Nanotechnology, Monitoring & Management*. 10 (2018). p. 366-379.

LIU, Y., LIU, Y., LIAO, N., CUI, F., PARK, M. & KIM, H. (2015). Fabrication and durable antibacterial properties of electrospun chitosan nanofibers with silver nanoparticles. *International Journal of Biological Macromolecules*. 79 (2015). p. 638-643.

MAHALINGAM, S., WU, X. & EDIRISINGHE, M. (2017). Evolution of self-generating porous microstructures in polyacrylonitrile-cellulose acetate blended fibers. *Journal of Materials and Design*. 134 (2017). p. 259-271.

MATABOLA, K.P & MOUTLAOLI, R.M. (2013). The influence of electrospinning parameters on the morphology and diameter of poly(vinyledene fluoride) nanofibers- effect of sodium chloride. *Journal of Material Science*. 48. p. 5475–5482.

MATHPAL, M.C., TRIPATHI, A.K., SINGH, M.K., GAIROLA, S.P., PANDEY, S.N. & AGARWAL, A. (2013). Effect of annealing temperature on raman spectra of TiO_2 nanoparticles. *Journal of Chemical Physics Letters*. 555 (2013). p. 182-186.

MATULEVICIUS, J., KLIUCININKAS, L. & MARTUZEVICIUS, D. (2014). Electrospinning of cellulose acetate fibers from a ternary solvent system. *Journal of Chemija*. 25 (2). p. 125–129.

MOHEMAN, A., SARWAR ALAM, M. & MOHAMMED, A. (2015). Recent trends in electrospinning of polymer nanofibers and their applications in ultra-thin chromatography. *Journal Advances in Colloid and Interface Science.* 229. p. 1-24.

MOFOKENG, J.P. (2015). *Preparation and characterization of completely biodegradable polymer-titania nanocomposites.* Thesis, (PhD). University of the Free State. Kestell Road, Phuthaditjhaba, 9866.

MORE, D.S., MOLOTO, M.J., MOLOTO, N. & MATABOLA, K.P. (2015). TOPO-capped silver selenide nanoparticles and their incorporation into polymer nanofibers using electrospinning technique. *Materials Research Bulletin*. 65. p. 14-22.

MORTEZA, H., MOHAMMAD, H., MOHAMMAD, B.J., SAMAN, S.G., MOHAMMAD, K.F., FARZAD, S. & MARJAN, G. (2012). Antibacterial effect of tio2 nanoparticles on pathogenic strain of E. coli. *International Journal of Advanced Biotechnology and Research*. 3 (3). p. 621-624.

MUTUMA, B.K., SHAO, G.N., KIM, W.O. & KIM, H.T. (2015). Sol-gel synthesis of mesoporous anatase-brookite and anatase-brookite-rutile TiO_2 nanoparticles and their photocatalytic properties. *Journal of Colloid and Interface Science*. 442 (2015). p. 1-7.

NAKATA, K. & FUJISHIMA, A. (2012). TiO_2 photocatalysis: design and applications. *Journal of Photochemistry and Photobiology C: Photochemistry Reviews*. 13. p.169-189.

NAMITA, R. (2015). Methods of preparation of nanoparticles-a review. *International Journal of Advances in Engineering & Technology*. 7 (4). p. 1806-1811.

NITHYAA, N., BHOOPATHIA, G., MAGESHA, G. & KUMAR, C.D.N. (2018). Neodymium doped TiO_2 nanoparticles by sol-gel method for antibacterial and photocatalytic activity. *Journal of Materials Science in Semiconductor Processing*. 83 (2018). p. 70-82.

NISTICO, R., SCALARONE, D. & MAGNACCA, G. (2017). Sol-gel chemistry, templating and spin-coating deposition: a combine approach to control in a simple way the porosity of inorganic thin films/ coatings. *Journal of Microporous and Mesoporous Materials*. 248. p. 18-29.

NYAMUKAMBA, P., OKOH, O., TICHANWA, L. & GREYLING, C. (2016). Preparation of Titanium Dioxide Nanoparticles Immobilized on Polyacrylonitrile Nanofibres for the Photodegradation of Methyl Orange. *International Journal of Photoenergy*. p. 1-9.

OCWELWANG, A.R. (2012). *Photocatalytic activity and antibacterial properties of Ag/N-doped TiO_2 nanoparticles on PVAE-CS nanofibre support.* Dissertation, (MSc). University of Fort Hare. King Williams Town Road, Alice, 5700.

PILLAY, V., DOTT, C., CHOONARA, Y.E., TYAGI, C., TOMAR, L., KUMAR, P., DU-TOIT, L.C. & NDESENDO, V.M.K. (2013). A review of the effect of processing variables on the fabrication of electrospun nanofibers for drug delivery applications. *Journal of Nanomaterials*. 2013. p. 1-22.

RAFIEI, S., MAGHSOODLOO, M., SABERI, M., LOTFI, S., MOTAGHITALAB, V., NOROOZI, B. & HAGHI, A.K. (2014). New Horizons in modelling and simulation of electrospun nanofibers: a detailed review. Journal of cellulose chemistry and technology. 48 (5-6). p.

RAMESH, S. (2013). Sol-gel synthesis and characterization of $Ag_{3(2+x)}Al_xTi_{4-x}O_{11+\delta}$ ($0.0 \leq x \leq 1.0$) nanoparticles. *Journal of Nanoscience*. 2013. p. 1-9.

RAO, B.G., MUKHERJEE, D. & REDDY, B.M. (2017). Novel approaches for preparation of nanoparticles. *Journal of Nanostructure for Novel Therapy.* 2017. p. 1-36.

RAZI, A. & MERYAM, S. (2013). TiO_2 nanoparticles as an antibacterial agents against E. coli. *International Journal of Innovative Research in Science, Engineering and Technology*. 2 (8). p. 3569- 3574.

REDDY, K.M., SUNKARA, V.M. & REDDY A.R. (2002). Bandgap studies on anatase titanium dioxide nanoparticles. *Journal of Materials Chemistry and Physics*. 78 (2002). p. 239-245.

RENEKER, D.H. &YARIN, A.L. (2008). Electrospinning jets and polymer nanofibers. *Journal of Polymer*. 49 (2008). p. 2387-2425.

RIAZ, T., AHMAD, A., SALEEMI, S., ADREES, M., JAMSHED, F., HAI, A.M. & JAMIL, T. (2016). Synthesis and characterization of polyurethane-cellulose acetate blend membrane for chromium (VI) removal, *Journal of Carbohydrate Polymers*. 153 (2016). p. 582-591.

RIZWAN, M., SINGH, M., MITRA, C.K. & MORVE, R.K. (2014). Ecofriendly application of nanomaterials: nanobioremediation. *Journal of Nanoparticles*. 2014. p. 1-7.

SABRIYE, P., ARZU, P. & MUGE, S.Y. (2013). Antimicrobial activity of synthesised TiO2 nanoparticles. *International Conference on Emerging Trends in Engineering and Technology*. 2013. p. 91-94.

SE WOOK, K., SEONG OK, H., I NA, S., JA YOUNG, C., & WON HO, P. (2015). Fabrication and characterization of cellulose acetate/montmorillonite composite nanofibers by electrospinning. *Journal of Nanomaterials.* p. 1-8

SEEMA, S., HARI, M. & PRADOM, K.S. (2013). Polymer- supported titanium dioxide photocatalysts for environmental remediation: a review. *Journal of Applied Catalysis A: General*. 462 (463). p. 178-195.

SHARMILA, D.R., VENCKATESH, R. & RAJESHWARI S. (2013). Synthesis of titanium dioxide nanoparticles by sol-gel technique. *International Journal of Innovative Research in Science, Engineering and Technology.* 3 (8). p. 15206-15211.

SHAUKAT, K., MAZHAR, U., WALEED, A.K., MUHAMMAD, W.U. & JOONG, K.P. (2015). Bacterial cellulose-titanium dioxide nanocomposites: nanostructural characteristics, antibacterial mechanism, and biocompatibility. *Journal of Cellulose*. 22. p. 565–579.

SILKE, M., JEAN, S.S., BRUCE CHASE, D. & RABOLT, J.F. (2002). Micro- and nanostructured surface morphology on electrospun polymer fibers. *Journal of Macromolecules.* 35. p. 8456-8466.

SON, W.K., YOUK, J.H., LEE, T.S. & PARK, W.H. (2004). Preparation of antimicrobial ultrafine cellulose acetate fibers with silver nanoparticles. *Journal of Macromolecular and Rapid Communictions*. 25 (2004). p. 1632–1637.

SOOKWAN, L., AMIR, R., KUN, W., KAREN, H., XIWANG, Z. &HUANTING, W. (2014). TiO_2 based photocatalytic membranes: a review. *Journal of Membrane Science*. 472. p.167-184.

SHI, Y., LI, Y., ZHANG, J., YU, Z. & YANG, D. (2015). Electrospun polyacrylonitrile nanofibers loaded silver nanoparticles by silver mirror reaction. *Journal of Materials Science and Engineering: C*. 51. p. 346-355.

TANG, Z., HE, C., TIAN, H., DING, J., HSIAO, B.S., CHU, B.J. & CHEN, H. (2016). Polymeric nanostructured materials for biomedical applications. *Journal of Progress in Polymer Science*. 60 (2016). p. 86-128.

TARUS, B., FADEL, N., AL-OUFY, A. & EL-MESSIRY, M. (2016). Effect of polymer concentration on the morphology and mechanical characteristics of electrospun cellulose acetate and poly (vinyl chloride) nanofiber mats. *Alexandria Engineering Journal*. 55 (2016). p. 2975-2984.

TAYADE, R.J., SUROLIA, P.K., KULKARNI, R.G. & JASRA, R.V. (2007). Photocatalytic degradation of dyes and organic contaminants in water using nanocrystalline anatase and rutile TiO_2. *Journal of Science and Technology of Advanced Materials*. 8 (2007). p.455-462.

THANDAVAMOORTHY, S., BHAT, G. S., TOCK, R. W., PARAMESWARAN, S. & RAMKUMAR, S. S. (2004). Electrospinning of nanofibers. *Journal of Applied Polymer Science*. 96. p. 557–569.

TUCK, S.J., LEACH, M.K., FENG, Z. & COREY, J.M. (2012). Critical variables in the alignment of electrospun PLLA nanofibers. *Journal of Materials Science and Engineering C*. 32 (2012). p.1779-1784.

VASHISTH, P., PRUTHI, P.A., SINGH, R.P. &PRUTHI, V. (2014). Process optimization for fabrication of gellan based electrospun nanofibers. *Journal of Carbohydrate Polymers*. 109 (2014). p. 16-21.

WAHABA, J. A. GIANCHANDANIB, P.K., KIMC, I.S. & NID, Q. (2018). Sonication induced effective approach for coloration of compact polyacrylonitrile (PAN) nanofibers. *Journal of Ultrasonics – Sonochemistry*. 10 (2018). p. 1-7.

WANG, G., XU, L., ZHANG, J., YIN, T. & HAN, H. (2011). Enhanced photocatalytic activity of TiO_2 powders (P25) via calcination treatment. *International Journal of Photoenergy*. 2012. p. 1-9.

WANG, T. & KUMAR, S. (2005). Electrospinning of Polyacrylonitrile Nanofibers. *Journal of Applied Polymer Sciences*. 102 (2006). p. 1023–1029.

WATANABE, N., KANEKO, T., UCHIMARU, Y., YANAGIDA, S, YASUMORI, A. & SUGAHARA Y. (2013). Preparation of water dispersible TiO_2 nanoparticles from titanium tetrachloride using urea hydrogen peroxide as an oxygen donor. *Journal of Crystal Engineering Communications*. 15. p. 10533–10540.

WETCHAKUN, N., INCESSUNGVORN, B., WETCHAKUN, K. & PHANICHPHANT, S. (2012). Influence of calcination temperature on anatase to rutile phase transformation in TiO_2 nanoparticles synthesised by the modified sol-gel method. *Journal of Materials Letters*. 82 (2012). p. 195-198.

XIAOMIN, S., WEIPING, Z., DELONG, M., QIAN, M., DENZEL, B., YING, M. &ANMING, H. (2015). Electrospinning of nanofibers and their applications for energy devices. *Journal of Nanomaterials*. 2015. p. 1-20.

YANG, S., JIN, R., HE, Z., QIAO, Y., SHI, S., KONG, W., WANG, Y. & LIU, X. (2017). An experimental study on the degradation of methyl orange by combining hydrodynamic cavitation and chlorine dioxide treatments. *Journal of Chemical Engineering*. 59 (2017). p. 289-295.

YORDEM, O.S., PAPILA, M. &MENCELOGLU, Y.Z. (2008). Effect of electrospinning parameters on polyacrylonitrile nanofiber diameter: An investigation by response surface methodology. *Journal of Materials and Design*. 29 (2008). p. 34–44.

ZARGHAM, S., BAZGIR, S., TAVAKOLI, A., RASHIDI, A.S. & DAMERCHELY, R. (2012). The effect of flow rate on morphology and deposition area of electrospun nylon 6 nanofiber. *Journal of Engineered Fibers and Fabrics*. 7 (4). p. 42-49.

ZHOU, M., YA, J., LUI, S., ZHAI, P. & JIANG, Z. (2008). Effects of calcination temperature on photocatalytic activity of SNO2/TiO2 composite films prepared by an EPD method. *Journal of Hazardous Materials*. 154 (2008). p. 1141-1148.

ZHOU, Z., LIN, W. & WU, X. (2016). Electrospinning ultrathin continuous cellulose acetate fibers for high-flux water filtration. *Journal of Colloids and Surface A: Physicochemical and Engineering Aspects*. 494 (2016). p. 21-29.

ZIZOVICA, I., SENEROVICC, L., MORICC, I., ADAMOVICD, T., JOVANOVICA, M., KRUSICA, M.K., MISICE, D., STOJANOVICA, D. & MILOVANOVICA, S. (2018). Utilization of supercritical carbon dioxide in fabrication of cellulose acetate films with anti-biofilm effects against *Pseudomonas aeruginosa* and *Staphylococcus aureus*. *The Journal of Supercritical Fluids*.140 (2018). p. 11-20.